

Inhomogeneous quenches as state preparation in two-dimensional conformal field theories

Masahiro Nozaki,^{1,2,*} Kotaro Tamaoka^{3,†} and Mao Tian Tan^{4,‡}

¹*Kavli Institute for Theoretical Sciences, University of Chinese Academy of Sciences, Beijing 100190, China*

²*RIKEN Interdisciplinary Theoretical and Mathematical Sciences (iTHEMS), Wako, Saitama 351-0198, Japan*

³*Department of Physics, College of Humanities and Sciences, Nihon University, Sakura-josui, Tokyo 156-8550, Japan*

⁴*Asia Pacific Center for Theoretical Physics, Pohang, Gyeongbuk, 37673, Korea*



(Received 14 March 2024; accepted 28 May 2024; published 20 June 2024)

The nonequilibrium process where the system does not evolve to the featureless state, that without quantum properties, is one of the new central objects in the nonequilibrium phenomena. In this paper, starting from the short-range entangled state in the two-dimensional conformal field theories (2D CFTs), the boundary state with a regularization, we evolve the system with the inhomogeneous Hamiltonians called Möbius/sine-square-deformed (SSD) ones. Regardless of the details of CFTs considered in this paper, during the Möbius evolution, the entanglement entropy exhibits the periodic motion called quantum revival. During SSD time evolution, except for some subsystems, in the large time regime, entanglement entropy and mutual information are approximated by those for the vacuum state. We argue the time regime for the subsystem to cool down to vacuum one is $t_1 \gg \mathcal{O}(L\sqrt{l_A})$, where t_1 , L , and l_A are time, system, and subsystem sizes. This finding suggests the inhomogeneous quench induced by the SSD Hamiltonian may be used as the preparation for the approximately vacuum state. We propose the gravity dual of the systems considered in this paper, furthermore, and generalize it. In addition to them, we discuss the relation between the inhomogeneous quenches and continuous multiscale entanglement renormalization ansatz (cMERA).

DOI: [10.1103/PhysRevD.109.126014](https://doi.org/10.1103/PhysRevD.109.126014)

I. INTRODUCTION

A major trend in twenty-first-century theoretical physics is the extensive utilization of quantum information-theoretic ideas and techniques in a wide range of seemingly disparate subfields of theoretical physics. For example, in the study of holography [1], an understanding of the quantum mechanical properties possessed by the system is expected to lead to a deeper grasp of the subject [2,3]. One such quantum information-theoretic concept is that of quantum error correction which originated from the field of quantum computing but has since been used for bulk reconstruction in holography [4,5] as well as the study of measurement-induced phase transition [6,7] by the

condensed matter community. Another topic from the field of quantum computation that might be of relevance to condensed matter physics is the preparation of quantum states [8–27]. In particular, obtaining low entropy states will allow the simulation of exotic phases of matter ranging from antiferromagnetic spin liquids to high-temperature superconductors [28,29]. One of the desired outcomes of state preparation is the preparation of these states faster than an adiabatic evolution of the system. In holography, preparing quantum states corresponds to the production of asymptotically AdS spacetimes.

Since two-dimensional conformal field theories (2D CFTs) possess the infinite-dimensional Virasoro symmetry, they may allow an analytic treatment of vacuum state preparation. In this paper, we consider the inhomogeneous quenches induced by the so-called Möbius and sine-squared deformed (SSD) Hamiltonians in 2D CFTs [30–46] and explore the utility of these quenches in vacuum state preparation. The densities of these inhomogeneous Hamiltonians are modulated by envelope functions that vary in space. In addition, these inhomogeneous Hamiltonians can be thought of as the Hamiltonians of systems that exist on a curved spacetime described by a metric whose time

*mnozaki@ucas.ac.cn

†tamaoka.kotaro@nihon-u.ac.jp

‡maotian.tan@apctp.org

Published by the American Physical Society under the terms of the Creative Commons Attribution 4.0 International license. Further distribution of this work must maintain attribution to the author(s) and the published article's title, journal citation, and DOI. Funded by SCOAP³.

component is determined by the envelope function. Originally, the modulation of energy density was used to remove the effect of the boundaries of spin systems with finite size [47–49]. Subsequently, these inhomogeneous deformations were generalized to 2D CFTs [50–56]. These inhomogeneous Hamiltonians were used in the implementation of 2D Floquet CFTs [35,36,40,41,57,58]. In addition, they have also been used to explore a variety of nonequilibrium phenomena and quantum information-theoretic aspects of 2D CFTs [59–64] and non CFTs [65].

In [32], the authors found that the time evolution induced by the SSD Hamiltonian can be used to approximately prepare the vacuum state. In the setup considered in [32], the system begins in the thermal state and subsequently undergoes time evolution with the SSD Hamiltonian which has a spatial point where the envelope function vanishes. If the subsystem does not include this point, the entanglement entropy associated with this subsystem evolves to that of the vacuum state. Regardless of the spatial location and the size of subsystems, the mutual information evolves into the mutual information for the vacuum state. In [66], this setup is generalized to a Floquet time evolution, and the authors consider the cooling effect of the inhomogeneous Hamiltonian.

In previous studies, the SSD time evolution was found to deform the entanglement structure of the long-range entangled state, where the entanglement entropy is proportional to the subsystem size, so that the resulting reduced density matrix is approximately given by that of the vacuum state. In this paper, we will explore whether this vacuum entanglement structure emerges during time evolution with the SSD Hamiltonian, starting from a short-range entangled state. The short-range entangled state considered in this paper is the regularized boundary state [67,68]. Since short-range entangled states are easily prepared in the laboratory, this study may pave the way for creating low entropy states using quantum quenches.

A. Summary

In this paper, starting from a short-range entangled state which we take to be the regulated boundary state, we evolve the system with Möbius/SSD Hamiltonians in 2D CFTs. The major difference from previous studies [8,9] is that we aim to explore whether vacuum states occur in CFTs with differing ability to scramble information which may determine the speed of information processing [69]. Our findings are as follows: *Entanglement entropy*: During Möbius time evolution, the time dependence of entanglement entropy exhibits a periodic behavior in time called quantum revival. During the SSD time evolution, when the edges of subsystems are not located at the origin, regardless of the spatial location of the subsystems, at sufficiently late times, the entanglement entropies are approximated by that of the vacuum state. As we will see, during the SSD time evolution, a local operator placed at the origin does not move, but local operators placed away from the origin will

move away from it. Hence, the origin is a fixed point under SSD time evolution. If the subsystem size, l_A , is much smaller than the system size, L , the time regime for the entanglement entropy for the single intervals to cool down to the vacuum one is $t_1 \gg t_* \approx \mathcal{O}(L\sqrt{l_A/\epsilon})$, where t_1 and ϵ are time and the parameter determining the short-range entanglement of the initial state. We argue that t_* characterizes the time for the subsystem to cool down to the vacuum one for the SSD time evolution. In addition, when the edges of subsystems are located at the origin, for sufficiently large times, the entanglement entropy logarithmically grows with time in the holographic CFTs while it approaches the saturation value with a power law in the free fermion CFTs. *Mutual information*: During the SSD time evolution, in the large time regime, mutual information eventually saturates to that of the vacuum one for both the free fermion CFT and the holographic CFTs while it goes to zero in the quasiparticle picture. This indicates that nonlocal correlations emerge under time evolution by these inhomogeneous Hamiltonians. The time dependence of entanglement entropy and mutual information suggests that the SSD time evolution prepares the state with the entanglement structure and nonlocal correlations possessed by the vacuum state. *Gravity dual*: We propose the gravity dual of the system considered and also generalize it. In particular, the end of the world brane approaches the asymptotic boundary and eventually collides with the cutoff surface. We argue that this is a timescale over which holographic calculations become unreliable. Furthermore, we discuss an interpretation of the Möbius/SSD time evolution as a type of tensor network called the continuous multiscale entanglement renormalization ansatz (cMERA).

B. Organization of this paper

In Sec. II, we will describe the details of the inhomogeneous quench, how to compute entanglement entropy in the twist operator formalism, and the evolution of local operators induced by the Möbius/SSD Hamiltonians. In Sec. III, we will present the time evolution of entanglement entropy in the 2D Dirac fermion CFT and in the quasiparticle picture that captures the dynamics of entanglement in the Dirac fermion CFT, as well as the entanglement entropy for the single interval in the 2D holographic CFTs which possess a gravitational dual. In Sec. IV, we will report the time evolution of mutual information in 2D CFTs considered in this paper. In Sec. V, we will present the gravity dual of the systems considered and give an interpretation of the quenches as a cMERA tensor network. In Sec. VI, we discuss the relation between the inhomogeneous quenches and renormalization group, and comment on future directions.

II. INHOMOGENEOUS QUENCHES FROM THE BOUNDARY STATE

Here, we will describe the inhomogeneous quenches considered in this paper. Suppose that we prepare the

system in the boundary state with a proper regularization, $e^{-\epsilon H}|\Psi_0\rangle$, [67] and then evolve it with inhomogeneous Hamiltonian H_{Inho} :

$$|\Psi(t)\rangle = \mathcal{N} e^{-itH_{\text{Inho}}} e^{-\epsilon H} |\Psi_0\rangle, \quad (2.1)$$

where \mathcal{N}^2 is the normalization constant that guarantees that $\langle\Psi(t)|\Psi(t)\rangle = 1$. The operator H is the homogeneous Hamiltonian defined as $H = \int_0^L dx h(x)$, where $h(x)$ is Hamiltonian density and L is the system size. One of the inhomogeneous Hamiltonians considered in this paper is the Möbius Hamiltonian defined as [36,57,58,70,71],

$$H_{\text{Möbius}} = \int_0^L dx \left[1 - \tanh(2\theta) \cos\left(\frac{2\pi x}{L}\right) \right] h(x), \quad (2.2)$$

where θ is a real parameter. The system considered in this paper is on the spatial circle with the circumference L . For $\infty > \theta > 0$, $H_{\text{Inho}} = H_{\text{Möbius}}$ is called Möbius Hamiltonian, and in the SSD limit where $\theta \rightarrow \infty$, it reduces to so-called sine-squared deformed Hamiltonian (SSD Hamiltonian) defined as

$$H_{\text{SSD}} = \int_0^L dx 2\sin^2\left(\frac{\pi x}{L}\right) h(x). \quad (2.3)$$

On the other hand, when $\theta = 0$, $H_{\text{Möbius}}$ reduces to the homogeneous Hamiltonian. In this paper, by using the time dependence of entanglement entropy and mutual information during the evolution induced by the Möbius/SSD Hamiltonian in the two-dimensional conformal field theories (2D CFTs), we will explore the entanglement structure of the state. The entanglement entropy and mutual information are defined as the von Neumann entropy for the reduced density matrix and a linear combination of the entanglement entropies respectively. Denote the density matrix of the state as $\rho(t) = |\Psi(t)\rangle\langle\Psi(t)|$. Divide the Hilbert space into A and its complement \bar{A} , and define the reduced density matrix associated to A as $\rho_A(t) = \text{tr}_{\bar{A}}\rho(t)$. The entanglement entropy for A is defined as the von Neumann entropy of $\rho_A(t)$,

$$S_A(t) = -\text{tr}_A \rho_A(t) \log \rho_A(t). \quad (2.4)$$

Let us now turn to the detailed definition of mutual information. Divide the Hilbert space into $A \cup B$ and $\bar{A} \cup \bar{B}$, define the entanglement entropies associated with A , B , and $A \cup B$, and define the mutual information as the

linear combination of these entanglement entropies,

$$I_{A,B} = S_A + S_B - S_{A \cup B}, \quad (2.5)$$

where S_A , S_B , and $S_{A \cup B}$ are the entanglement entropies associated with A , B and $A \cup B$.

The parameter region considered in this paper The parameter regime where we explore the inhomogeneous nonequilibrium process in this paper is

$$L \gg l_{\mathcal{V}}, t_1 \gg \epsilon \gg 1, \quad (2.6)$$

where $l_{\mathcal{V}}$ denotes the size of the subsystem \mathcal{V} and t_1 is the time associated with the Möbius/SSD Hamiltonian.

A. Entanglement entropy in the twist operator formalism

To employ the Euclidean path-integral formalism suitable to the analytical computation of the entanglement entropy in 2D CFTs, we define the Euclidean density operator as

$$\rho_E = \mathcal{N}^2 e^{-\tau_1 H_{\text{Inho}}} e^{-\epsilon H} |\Psi_0\rangle\langle\Psi_0| e^{-\epsilon H} e^{\tau_1 H_{\text{Inho}}}, \quad (2.7)$$

where ϵ is a regularization parameter, and τ_1 is a real Euclidean time. The normalization parameter \mathcal{N} guarantees that $\text{tr}\rho_E = 1$, and it satisfies $\mathcal{N}^{-2} = \langle\Psi_0|e^{-2\epsilon H}|\Psi_0\rangle$.

Divide the Hilbert space into \mathcal{V} and $\bar{\mathcal{V}}$, the complement space to \mathcal{V} , and then define a reduced Euclidean density matrix associated with \mathcal{V} as $\rho_{E,\mathcal{V}} = \text{tr}_{\bar{\mathcal{V}}}\rho_E$. Subsequently, define Euclidean entanglement entropy of \mathcal{V} as the von Neumann entropy of $\rho_{E,\mathcal{V}}$:

$$\begin{aligned} S_{E,\mathcal{V}} &= \lim_{n \rightarrow 1} S_{E,\mathcal{V}}^{(n)} = \lim_{n \rightarrow 1} \frac{1}{1-n} \log [\text{tr}_{\mathcal{V}} \rho_{E,\mathcal{V}}^n] \\ &= -\text{tr}_{\mathcal{V}} [\rho_{E,\mathcal{V}} \log \rho_{E,\mathcal{V}}], \end{aligned} \quad (2.8)$$

where we call $S_{E,\mathcal{V}}^{(n)}$ the n th Rényi entanglement entropy. In the path-integral formalism, n th Rényi entanglement entropy is given by $\text{tr}_{\mathcal{V}} \rho_{E,\mathcal{V}}^n$ which is the partition function on a n -sheeted geometry where each of sheets is a finite cylinder.

Let us assume that \mathcal{V} is a single interval. In the twist operator formalism, $\text{tr}_{\mathcal{V}} \rho_{E,\mathcal{V}}^n$ is given by the two-point function of the twist and antitwist operators. As a consequence, the n th Rényi entanglement entropy is given by

$$S_{E,\mathcal{V}}^{(n)} = \frac{1}{1-n} \log \left[\frac{\langle\Psi_0|e^{-\epsilon H} e^{\tau_1 H_{\text{Inho}}} \mathcal{T}_n(v_1) e^{-\tau_1 H_{\text{Inho}}} e^{\tau_1 H_{\text{Inho}}} \bar{\mathcal{T}}_n(v_2) e^{-\tau_1 H_{\text{Inho}}} e^{-\epsilon H} |\Psi_0\rangle}{\langle\Psi_0|e^{-2\epsilon H} |\Psi_0\rangle} \right], \quad (2.9)$$

where v_1 and v_2 denote the edges of \mathcal{V} , respectively. Here, \mathcal{T}_n and $\bar{\mathcal{T}}_n$ are the primary operators called the twist and anti-twist operators. Their conformal dimensions are $(h_n, \bar{h}_n) = (\frac{c}{24}(n - \frac{1}{n}), \frac{c}{24}(n - \frac{1}{n}))$. Here, we assume that $L > v_1 > v_2 > 0$. As in [32], the evolution of the primary operator $\mathcal{O}(w, \bar{w})$ induced by Möbius/SSD Hamiltonian is given by

$$e^{\tau_1 H_{\text{Inho}}} \mathcal{O}(w, \bar{w}) e^{-\tau_1 H_{\text{Inho}}} = \left(\frac{dw^{\text{New}, \alpha=0,1}}{dw} \right)^{h_n} \left(\frac{d\bar{w}^{\text{New}, \alpha=0,1}}{d\bar{w}} \right)^{\bar{h}_n} \times \mathcal{O}(w^{\text{New}, \alpha=0,1}, \bar{w}^{\text{New}, \alpha=0,1}), \quad (2.10)$$

where $(w^{\text{New}, \alpha=0,1}, \bar{w}^{\text{New}, \alpha=0,1})$ is the location of the operator during the Euclidean time evolution induced by the Möbius ($\alpha = 1$) and SSD ($\alpha = 0$) Hamiltonians, respectively. The details of the operator trajectory and the operator position $(w^{\text{New}, \alpha}, \bar{w}^{\text{New}, \alpha})$ are reported in Appendices A 1 and A 2. The Euclidean Rényi entanglement entropy is given by the “free energy” of the two point function on the finite cylinder where the length along Euclidean time is 2ϵ , and the circumference of the spatial circle is L ,

$$S_{E, \mathcal{V}}^{(n)} = \frac{h_n}{1-n} \log \left[\prod_{i=1,2} \left(\frac{dw_{v_i}^{\text{New}, \alpha}}{dw_{v_i}} \right) \left(\frac{d\bar{w}_{v_i}^{\text{New}, \alpha}}{d\bar{w}_{v_i}} \right) \right] + \frac{1}{(1-n)} \log \left[\frac{\langle \Psi_0 | e^{-2\epsilon H} \mathcal{T}_n(w_{v_1}^{\text{New}, \alpha} + \epsilon, \bar{w}_{v_1}^{\text{New}, \alpha} + \epsilon) \bar{\mathcal{T}}_n(w_{v_2}^{\text{New}, \alpha} + \epsilon, \bar{w}_{v_2}^{\text{New}, \alpha} + \epsilon) | \Psi_0 \rangle}{\langle \Psi_0 | e^{-2\epsilon H} | \Psi_0 \rangle} \right]. \quad (2.11)$$

In the von Neumann limit where $n \rightarrow 1$, the Euclidean Rényi entanglement entropy reduces to the Euclidean entanglement entropy,

$$S_{E, \mathcal{V}} = -\frac{c}{12} \log \left[\prod_{i=1,2} \left(\frac{dw_{v_i}^{\text{New}, \alpha}}{dw_{v_i}} \right) \left(\frac{d\bar{w}_{v_i}^{\text{New}, \alpha}}{d\bar{w}_{v_i}} \right) \right] + \lim_{n \rightarrow 1} \frac{1}{(1-n)} \log \left[\frac{\langle \Psi_0 | e^{-2\epsilon H} \mathcal{T}_n(w_{v_1}^{\text{New}, \alpha} + \epsilon, \bar{w}_{v_1}^{\text{New}, \alpha} + \epsilon) \bar{\mathcal{T}}_n(w_{v_2}^{\text{New}, \alpha} + \epsilon, \bar{w}_{v_2}^{\text{New}, \alpha} + \epsilon) | \Psi_0 \rangle}{\langle \Psi_0 | e^{-2\epsilon H} | \Psi_0 \rangle} \right]. \quad (2.12)$$

In this paper, we will explore the time dependence of the entanglement entropy for the single interval in 2D massless free fermion and holographic CFTs. To make it easier to grasp the key points of the analysis, the details of the calculation of the entanglement entropy for a single interval are postponed to Appendix B.

B. The trajectory of the local operator during the time evolution induced by SSD/Möbius evolution

After performing the analytic continuation, $\tau_1 = it_1$, we consider the trajectory of the twist and anti-twist operators during the time evolution induced by the SSD/Möbius

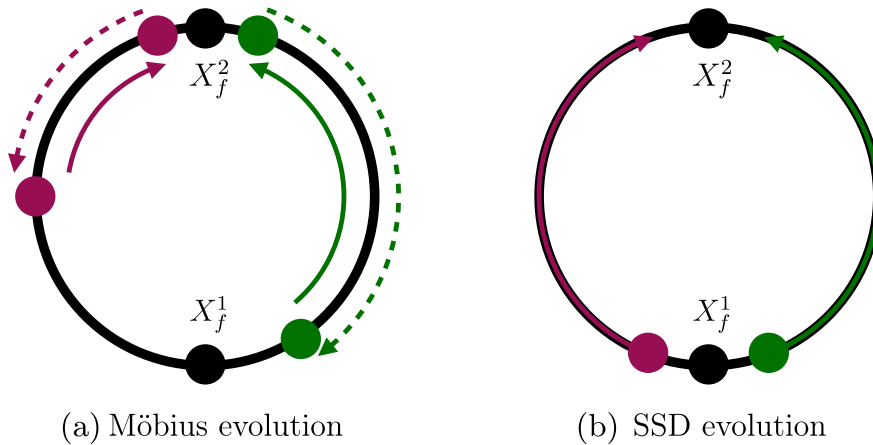


FIG. 1. The evolution of operators during the evolution induced by SSD/Möbius Hamiltonian. The black dots illustrate the fixed point of H_{SSD} . The green (purple) dot illustrates the operator that is initially inserted at $L/2 > x > 0$ ($L > x > L/2$) and $t_1 = 0$, and its trajectory during the time evolution is illustrated by the green (purple) curve. In (a), we show the evolution of operators during the Möbius time evolution. In (b), we show the evolution of operators during the SSD time evolution.

Hamiltonian. Define the spatial position of these operators in the Heisenberg picture as

$$X_{v_i}^{\text{New},\alpha} = \frac{W_{v_i}^{\text{New},\alpha} - \bar{w}_{v_i}^{\text{New},\alpha}}{2i}, \quad (2.13)$$

where v_i is the insertion point of these operators in the Schrödinger picture. If these operators are inserted at $v_i = 0, L/2$, then during the SSD time evolution, $X_{v_i}^{\text{New},\alpha}$ does not vary in time. Therefore, call them fixed points, and let X_f^1 and X_f^2 denote 0 and $L/2$, respectively. During the Möbius evolution, these operators in the Heisenberg picture periodically move in time between X_f^1 and X_f^2 (see (a) of Fig. 1), while during the SSD evolution, those move to X_f^2 and accumulate around that spatial point (see (b) of Fig. 1). Consequently, if the subsystem is a single interval including X_f^1 , then during the SSD evolution, the effective subsystem size in the Heisenberg picture defined as $V_{\text{eff}} = X_{v_1}^{\text{New},\alpha} - X_{v_2}^{\text{New},\alpha}$, monotonically grows with time. If the subsystem is a single interval excluding X_f^1 , then during the SSD evolution, $V_{\text{eff}} = X_{v_1}^{\text{New},\alpha} - X_{v_2}^{\text{New},\alpha}$ eventually shrinks with time.

III. THE TIME DEPENDENCE OF ENTANGLEMENT ENTROPY IN 2D CFTs

In this section, we will report the time dependence of entanglement entropy in 2D CFTs.

A. The time evolution of entanglement entropy in 2D free fermion

As examples of nonchaotic dynamics, we compare the Rényi entropy of a single interval in the free fermionic CFT as well as in the quasiparticle picture which will be discussed later in Sec. III B. The plots for different subsystems centered at different points along the spatial circle are shown in Fig. 2. Let us just summarize the salient points of these plots. First, the CFT result and the quasiparticle entanglement agree to the leading order in $\frac{1}{\epsilon}$. The subleading difference is most apparent when the Rényi entropy after a SSD quench decays to the vacuum value for the CFT when the subsystem does not end on X_f^1 but it decays to zero for the quasiparticles since the left and right moving quasiparticles will accumulate on opposite sides of the fixed point X_f^1 at late times and hence the entanglement entropy will asymptotically decay to zero. The behavior of these free theories during Möbius evolution is very similar to that for the holographic CFTs except for the fact that the entanglement entropy of quasiparticles drops down to zero at integer multiples of $\frac{L}{2} \cosh 2\theta$ and the entanglement entropy of the free fermion CFT similarly drop down to a small value. The entanglement entropy of

quasiparticles must decay back to zero at integer multiples of $L \cosh 2\theta$ because the quasiparticles return to their initial positions at those times. At half-integer multiples of $\frac{L}{2} \cosh 2\theta$, the left and right moving partners of each Bell pair meet up and so give no contribution to the entanglement entropy. Secondly, the plots for both boundary conditions for the free fermion CFT appear to be identical. The boundary condition dependent terms in the free fermion CFT Rényi entropy are either zero or tiny compared to the total entropy in most cases except for the case where the interval ends exactly on the fixed point X_f^1 in which case the boundary condition-dependent component is actually larger than the boundary condition-independent part for the larger values of θ . In any case, the upshot is that the plots appear identical for both boundary conditions in the free fermion CFT and hence do not appear to depend on the boundary condition imposed on the Dirac fermions.

Just as in the holographic case, to obtain a nonzero value of the entanglement entropy for the quasiparticles and free fermion CFTs at late times, place the interval so that one of the endpoints sits exactly on the SSD fixed point X_f^1 so that exactly one member of each Bell pair in the quasiparticle picture is contained inside the subsystem at late enough times.

B. Quasiparticle picture

The quasiparticle picture for the uniform global quench [72–74] can be extended to the inhomogeneous case by assuming that the quasiparticle is not moving with uniform speed but instead with a speed that is determined by the inhomogeneous envelope function that appears in the inhomogeneous Hamiltonian. This might be due to the fact that the CFTs considered in this paper are defined on curved backgrounds where the time component of the metric, which determines the speed of moving objects, is given by the inhomogeneous envelope function. During the Möbius evolution, a quasiparticle that begins at position x_0 at time t_0 is located at x at time t_1 which is given by

$$\frac{\pi(t_1 - t_0)}{L \cosh 2\theta} = \pm \left[\tan^{-1} \left(e^{2\theta} \tan \frac{\pi x}{L} \right) - \tan^{-1} \left(e^{2\theta} \tan \frac{\pi x_0}{L} \right) \right] \quad (3.1)$$

where the $+$ ($-$) sign correspond to right(left) moving quasiparticles. For simplicity, set the initial time $t_0 = 0$.

For a subsystem A , which could generally be a union of intervals, the entanglement entropy as predicted by the quasiparticle picture is given by the number of Bell pairs shared between A and its complement. Let $x_{0,i}(x, t_1)$ be the initial position of a quasiparticle situated at position x at time t_1 , where $i = R, L$ denotes the chirality of the quasiparticles. For additional details, see Ref. [32]. Assuming that the quasiparticles are conserved, the right-moving and left-moving quasiparticles that are inside A at a given time

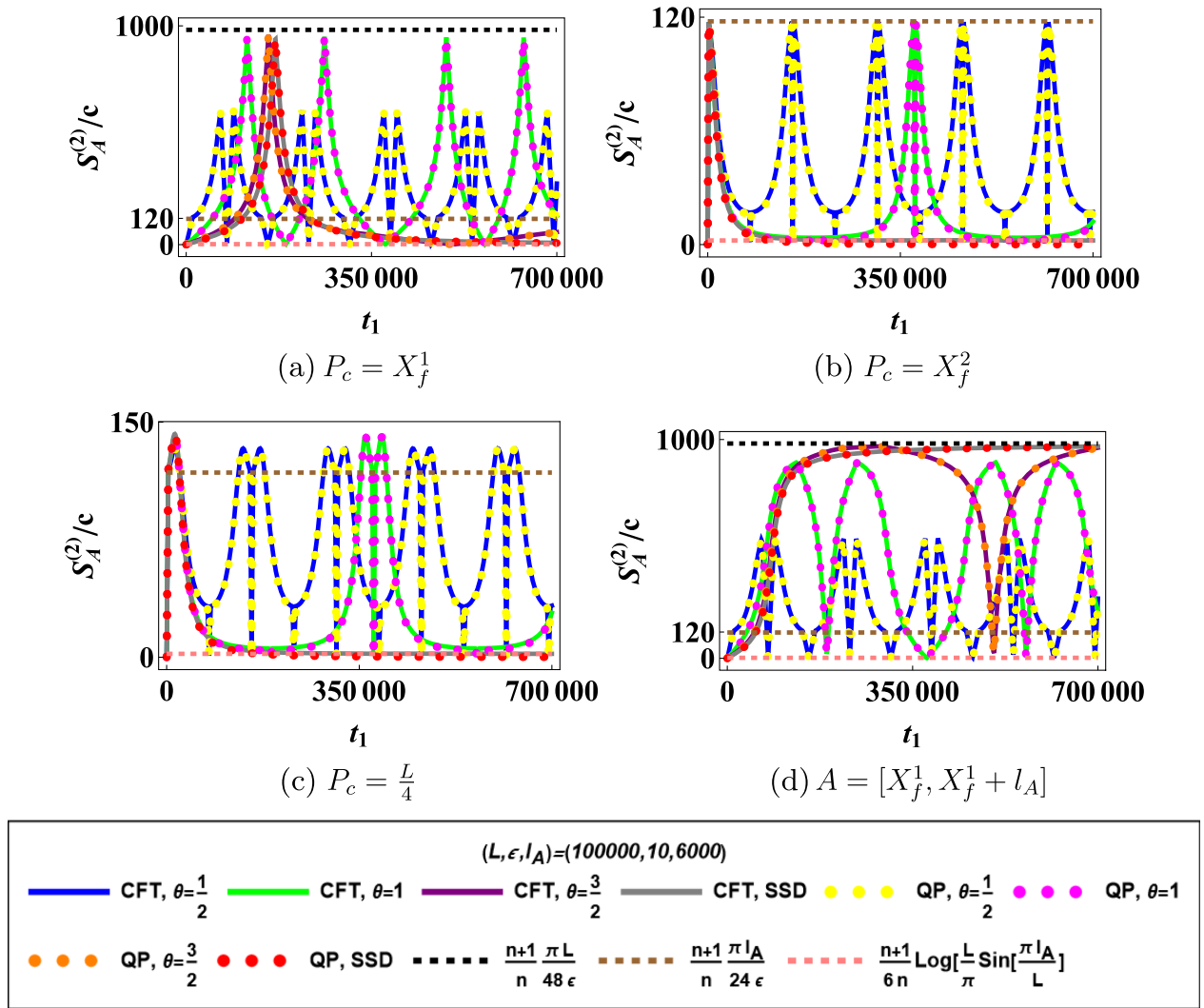


FIG. 2. Plots of the second Rényi entropy for the 2d free fermion CFT as well as the quasiparticle picture for a total system size of $L = 100000$, $\epsilon = 10$ and a subsystem size of $l_A = 6000$ with a center P_c located at various positions.

t_1 are therefore initially situated inside $x_{0,R}(A, t_1)$ and $x_{0,L}(A, t_1)$ at $t = 0$, respectively. A simple example for the uniform Hamiltonian is depicted in Fig. 3. Similarly, the left and right moving quasiparticles that end up in the

complement of A , \bar{A} , initially began in the subsystems $x_{0,L}(\bar{A}, t_1)$ and $x_{0,R}(\bar{A}, t_1)$, respectively.

While the distribution of quasiparticles after a time evolution with an inhomogeneous Hamiltonian is

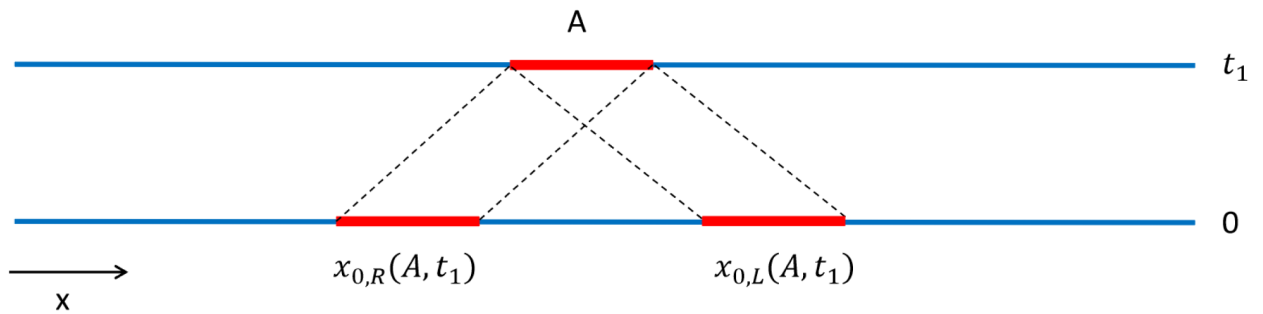


FIG. 3. For a given interval A , $x_{0,R}(A, t_1)$ and $x_{0,L}(A, t_1)$ are the intervals that will move respectively to the right and left and will coincide with A at time t_1 . Shown here is the simplest case where the Hamiltonian is uniform so the intervals are translated with unit speed.

complicated [32], the quasiparticles are initially distributed uniformly. Since the entanglement entropy of A is given by the Bell pairs that it shares with its complement, the entanglement entropy can simply be written as

$$S_A^{(n)}(t_1) = \rho_0^{(n)} [\text{length of } x_{0,L}(\bar{A}, t_1) \cap x_{0,R}(A, t_1) + \text{length of } x_{0,R}(\bar{A}, t_1) \cap x_{0,L}(A, t_1)] \quad (3.2)$$

where $\rho_0^{(n)} = \frac{n+1}{n} \frac{\pi c}{48\epsilon}$ can be fixed by equating the saturation value of $S_A^{(n)}$ for the uniform Hamiltonian for a single finite interval on the real line with the known CFT result [72] to leading order in $\frac{1}{\epsilon}$ and using the fact that for the uniform Hamiltonian, $x_{0,R}(A, t_1)$ and $x_{0,L}(A, t_1)$ are entirely contained inside $x_{0,L}(\bar{A}, t_1)$ and $x_{0,R}(\bar{A}, t_1)$ respectively at sufficiently late times.

The quasiparticle picture entanglement entropy appears to vanish when the time t_1 is a multiple of $\frac{L}{2} \cosh 2\theta$. This is obvious when t_1 is a multiple of $L \cosh 2\theta$ since all the quasiparticles would have returned to their original position so the entanglement entropy reverts back to its original value of 0. When t_1 is a half-integer multiple of $L \cosh 2\theta$, the quasiparticle entanglement entropy vanishes not because the quasiparticles have returned to their initial positions but because the left and right moving partners of each Bell pair have met up after traversing the spatial circle on opposite directions.

We can also compute the mutual information as predicted by the quasiparticle picture. The mutual information between two subsystems A and B is given by twice the number of Bell pairs that have one partner in each system since these Bell pairs contribute to both $S_A^{(n)}$ and $S_B^{(n)}$ but not to $S_{AB}^{(n)}$. Therefore,

$$I_{A,B}^{(n)}(t_1) = 2\rho_0^{(n)} [\text{length of } x_{0,L}(A, t_1) \cap x_{0,R}(B, t_1) + \text{length of } x_{0,R}(A, t_1) \cap x_{0,L}(B, t_1)]. \quad (3.3)$$

1. Late time behavior of free theories when the interval ends on X_f^1

The Rényi entropy for a subsystem that ends on the fixed point X_f^1 , $[0, X_1]$, in the quasiparticle picture is

$$S_A^{(n)t_1 \gg L} \approx \frac{n+1}{48n} \frac{\pi c L}{\epsilon} \left(1 - \frac{L}{\pi^2 t_1}\right). \quad (3.4)$$

In the late time regime of interest $t_1 \gg L \gg \epsilon$, the boundary condition-dependent terms in the free fermion CFT entanglement entropy are exponentially suppressed and the late time entanglement entropy of a single interval that ends on the fixed point when either boundary state is quenched by the SSD Hamiltonian is

$$S_{[0, X_1]}^{(n)}(t_1) \approx \frac{n+1}{6n} \log \left(\frac{L}{\pi} \sin \frac{\pi X_1}{L} \right) + \frac{n+1}{48n} \frac{\pi L}{\epsilon} \left(1 - \frac{2L}{\pi^2 t_1}\right), \quad t_1 \gg L \gg \epsilon, \frac{t_1}{L} \gg \frac{L}{\epsilon}. \quad (3.5)$$

This is very similar to the late-time behavior of the entanglement entropy of a single interval that ends on the fixed point X_f^1 for the quasiparticles undergoing a SSD quench. The only difference is the additional factor of 2 in the power law $\frac{1}{t_1}$ decay to the saturation value which is subleading in $\frac{L}{\epsilon}$. The saturation value also has the additional vacuum Rényi entropy which is zero in the quasiparticle case as discussed earlier.

The discrepancy between the quasiparticle entanglement entropy and the CFT Rényi entropy can be attributed to the order of the limits taken. The term that gives rise to late time saturation is

$$S_{[0, X_1]}^{(n)}(t_1) = \frac{n+1}{12n} \log \theta_1 \left(\frac{w_{X_1}^{\text{New}, \alpha} + \bar{w}_{X_1}^{\text{New}, \alpha}}{4\epsilon} \middle| i \frac{L}{4\epsilon} \right) + \dots \approx \frac{n+1}{12n} \frac{\pi L}{4\epsilon} \left(1 - \frac{L}{\pi^2 t_1}\right) + \frac{n+1}{12n} \log \left(1 + e^{-\frac{L^2}{2\epsilon\pi t_1}}\right) + \dots \quad (3.6)$$

If we first send $\frac{L}{\epsilon} \rightarrow \infty$ in (3.6)

$$S_{[0, X_1]}^{(n)}(t_1) \approx \frac{n+1}{48n} \frac{\pi L}{\epsilon} \left(1 - \frac{L}{\pi^2 t_1}\right) + \dots \quad (3.7)$$

This is the same answer as for the quasiparticles (3.4). On the other hand, if we first send $\frac{t_1}{L} \rightarrow \infty$ in (3.6), we get

$$S_{[0, X_1]}^{(n)}(t_1) \approx \frac{n+1}{48n} \frac{\pi L}{\epsilon} \left(1 - \frac{2L}{\pi^2 t_1}\right) + \dots \quad (3.8)$$

which corresponds to the asymptotic expression we found earlier. Therefore, we see that the discrepancy comes from the fact that the quasiparticles correspond to taking the $\epsilon \rightarrow 0$ limit of the CFT first and so would not truly capture the $t_1 \rightarrow \infty$ behavior of the CFT.

C. The time evolution of entanglement entropy in 2D holographic CFT

We focus on the analysis of the time dependence of entanglement entropy and mutual information in 2D holographic CFTs.

1. The analysis of nonuniversal piece

Now, we perform the analytic continuation to real time, $\tau_1 = it_1$, and report the time dependence of the nonuniversal piece of entanglement entropy in 2D holographic

CFTs. As explained in Sec. B 2, the time dependence of the nonuniversal piece is determined by that of the geodesic length on the BTZ black hole geometry. The t_1 -dependence of $S_{\mathcal{V};\text{con}}$ is determined by the length of the geodesic connecting the points at the different Euclidean time slices in the method of image. Without employing the method of the image, the t_1 -dependence of this geodesic length should be equal to that of the geodesic length ending at the end of the world brane (EoW) via the AdS/BCFT correspondence¹ [75,76]. In the high temperature regime, the location of EoW in the radial direction is near the boundary. In the parameter regime, where $v_1 - v_2 \gg \epsilon$, the geodesic length is given by the one ending at the EoW brane. Consequently, in the small time region, $t_p > t_1 > 0$, the t_1 -dependence of the nonuniversal piece of S_A is determined by the motion of the EoW. Here, we define t_p as the time when $S_{\mathcal{V};\text{dis}}$ exchanges the dominance with $S_{\mathcal{V};\text{con}}$. We will present the detailed motion of the EoW in Sec. V. We divide the system into A and \bar{A} , the complement to A , let $X_{i=1,2}$ denote the edges of A , and assume $L > X_1 > X_2 \geq 0$. We will report on the time dependence of entanglement entropy during the Möbius/SSD time evolution in the four cases: (1) $X_f^1 \in A$; (2) $L/2 > X_1 > X_2 > 0$; (3) $X_f^2 \in A$; (4) $X_2 = X_f^1$. In the cases considered in this paper, $S_{\mathcal{V};\text{con}}$ monotonically grows in time according to the motion of EoW [59]. For the large t_1 -regime, $t_1 > t_p$, the t_1 -dependence of the nonuniversal piece is determined by the trajectory of twist and antitwist operators during the time evolution induced by the inhomogeneous Hamiltonians. As a simple example, let us consider the t_1 -dependence of the nonuniversal piece for the reduced density matrix associated with the subsystem including X_f^1 during the evolution induced by H_{SSD} . In $t_p > t_1 > 0$, the t_1 -dependence of the nonuniversal piece is determined by that of $S_{\mathcal{V};\text{con}}$. In $t_1 > t_p$, the t_1 -dependence of the nonuniversal piece is determined by the smaller one of $S_{\mathcal{V};\text{dis},1}$ and $S_{\mathcal{V};\text{dis},2}$. We define an effective subsystem size in the Heisenberg picture as

$$V_{\text{eff}} = \begin{cases} L - (X_{v_1}^{\text{New},\alpha} - X_{v_2}^{\text{New},\alpha}) & \text{for } X_f^1 \notin \mathcal{V} \\ X_{v_1}^{\text{New},\alpha} - X_{v_2}^{\text{New},\alpha} & \text{for } X_f^1 \in \mathcal{V} \end{cases}. \quad (3.9)$$

In the time-regime where $L/2 > V_{\text{eff}}$, the nonuniversal piece is given by $S_{\mathcal{V};\text{dis},1}$, while in $V_{\text{eff}} > L/2$, it is determined by $S_{\mathcal{V};\text{dis},2}$.

2. During the Möbius/SSD time evolution

Now, let us present the time dependence of S_A during the Möbius/SSD time evolution. For all the cases considered,

¹We postpone detailed discussion of the AdS/BCFT correspondence until Sec. VA, but we will use both equivalent interpretations in this section as well. Readers unfamiliar with the AdS/BCFT correspondence may refer to the first part of Sec. VA in advance.

$S_{A;\text{con}}$ monotonically grows with time during the Möbius/SSD evolution (see Appendix C). The exchanging time $t_1 = t_p$ should be determined by

$$\begin{aligned} w_{X_1}^{\text{New},\alpha} + \bar{w}_{X_2}^{\text{New},\alpha} &= iL \quad \text{For } S_{\text{con}} = S_{\text{dis},1} (< S_{\text{dis},2}), \\ \bar{w}_{X_1}^{\text{New},\alpha} + w_{X_2}^{\text{New},\alpha} &= 0 \quad \text{For } S_{\text{con}} = S_{\text{dis},2} (< S_{\text{dis},1}). \end{aligned} \quad (3.10)$$

After $t_1 = t_p$, the nonuniversal piece of S_A is determined by $S_{\text{dis},i}$.

We depict S_A in cases (1), (2), and (3) as a function of t_1 in Fig. 4. During the Möbius evolution in the cases (1), (2), and (3), the time-dependence of S_A exhibits the two time regimes: a heating one for $0 < t < t_p$, and an oscillating one of $t_p < t$. In the heating regime, the growth of S_A depends on the inhomogeneous parameter θ , the subsystem size L_A , and the system size L . Regardless of time evolution considered, in the limit where $\pi(w_{X_i}^{\text{New},\alpha} + \bar{w}_{X_i}^{\text{New},\alpha})/4i\epsilon \gg 1$, the early time behavior of S_A should be determined by the nonuniversal piece of S_A ,

$$S_A \approx S_{A,\text{Nonuni}} \approx \frac{cL}{24\epsilon} \times \sum_{i=1,2} [\varphi_{X_i,\tau_i,\alpha} + \bar{\varphi}_{X_i,\tau_i,\alpha}], \quad (3.11)$$

where the details of φ and $\bar{\varphi}$ are reported in Appendix A 2. During the Möbius time evolution, $\varphi_{X_1,\tau_1,1} + \bar{\varphi}_{X_1,\tau_1,1}$ monotonically grows with time. In the time interval, $1 \gg \varphi_{X_i,\tau_i,0} + \bar{\varphi}_{X_i,\tau_i,0} \gg \frac{4\pi\epsilon}{L}$, the early-time growth of S_A is approximated by

$$S_A \approx \frac{c\pi t_1}{12\epsilon} \sum_{i=1,2} \left[1 - \tanh 2\theta \cos\left(\frac{2\pi X_i}{L}\right) \right]. \quad (3.12)$$

Thus, in this time interval, S_A linearly grows with t_1 as in the homogeneous quench [74,77]. However, the coefficient of the linear growth is given by multiplying that of the homogeneous quench by an additional factor of the envelope function, $1 - \tanh 2\theta \cos(\frac{2\pi X_i}{L})$. In the oscillating regime, S_A periodically behaves in time with the period $L \cosh 2\theta$. During the evolution induced by the SSD Hamiltonian ($\alpha = 0$), the time dependence of S_A exhibits the two time-regimes: a heating one for $0 < t < t_p$, and a cooling one for $t_p < t$. As in the case of the time evolution in cases (1), (2), and (3), S_A in the heating regime monotonically grows with t_1 . In the limit where $\pi(w_{X_i}^{\text{New},0} + \bar{w}_{X_i}^{\text{New},0})/4i\epsilon \gg 1$, the early time behavior of S_A is given by (3.11) for $\alpha = 0$. During the SSD time evolution, $\varphi_{X_i,\tau_i,0} + \bar{\varphi}_{X_i,\tau_i,0}$ monotonically increases with t_1 . In the time interval, $1 \gg \varphi_{X_i,\tau_i,0} + \bar{\varphi}_{X_i,\tau_i,0} \gg \frac{4\pi\epsilon}{L}$, the early-time growth of S_A is approximated by

$$S_A \approx \frac{c\pi t_1}{6\epsilon} \sum_{i=1,2} \sin^2\left(\frac{\pi X_i}{L}\right). \quad (3.13)$$

Thus, in this time interval, S_A linearly grows with t_1 . The coefficient of the linear growth is given by multiplying that

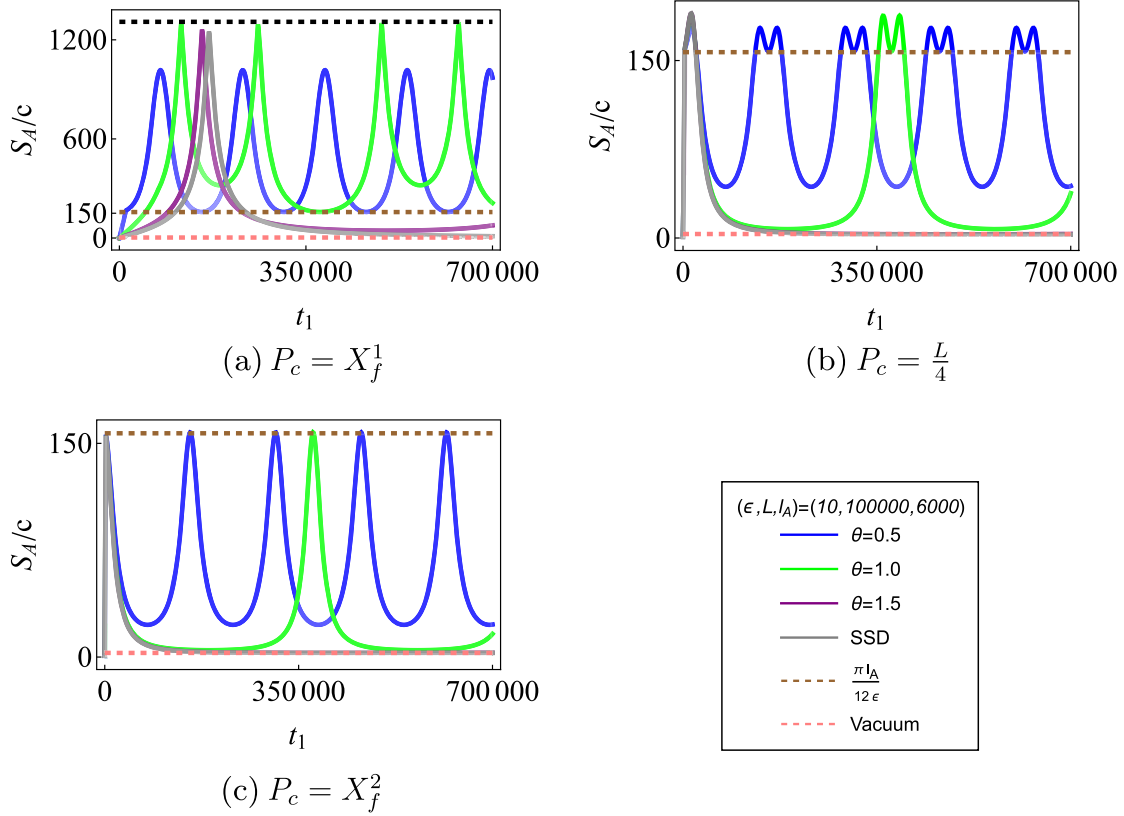


FIG. 4. The t_1 -dependence of S_A during the evolution induced by the Möbius and SSD Hamiltonians. The panels, [a], [b], and [c], correspond to cases (1), (2), and (3). Here, P_c denotes the center of A . For simplicity, in [a], [b], and [c], P_c is taken to be $P_c = X_f^1$, $L/4$, and X_f^2 , respectively. The black dashed line illustrates the entanglement entropy of the thermal state with 4ϵ , the inverse temperature, for half of the total space. The gray and pink dashed lines illustrate S_A of this thermal state and the vacuum state.

for homogeneous quench by the envelope function, $2 \sin^2(\frac{\pi X_i}{L})$. In the cooling regime, the universal and nonuniversal pieces of S_A are asymptotically given by

$$S_{A,\text{Uni}} \approx \frac{c}{3} \log \left[\frac{2\pi t_1 \sin(\frac{\pi X_1}{L})}{L} \right] + \frac{c}{3} \log \left[\frac{2\pi t_1 \sin(\frac{\pi X_2}{L})}{L} \right],$$

$$S_{A,\text{Nonuni}} \approx S_{\text{dis},2} \approx \frac{c}{3} \log \left[\frac{L}{\pi} \cdot \frac{L^2}{4\pi^2 t_1^2} \cdot \frac{\sin \left[\frac{\pi(X_1 - X_2)}{L} \right]}{\sin \left[\frac{\pi X_1}{L} \right] \sin \left[\frac{\pi X_2}{L} \right]} \right]. \quad (3.14)$$

Thus, the universal and nonuniversal pieces logarithmically grow and decrease with t_1 , respectively. Since the logarithmic growth cancels with the logarithmic decrease, S_A for large t_1 becomes independent of t_1 . As a consequence, S_A for the large t_1 is approximated by the vacuum entanglement entropy,

$$S_A = S_{A,\text{Uni}} + S_{A,\text{Nonuni}} \approx \frac{c}{3} \log \left[\frac{L}{\pi} \sin \left[\frac{\pi(X_1 - X_2)}{L} \right] \right]. \quad (3.15)$$

Unlike the case of the thermal state in [32], even if the subsystem includes $x = X_f^1$, the entanglement entropy saturates to that for the vacuum one, not the thermal one.

3. Thermal configuration

As in cases (1)-(3), if the edge of A is not at $x = X_f^1$, then S_A is asymptotically approximated by the vacuum entanglement entropy. Now, we consider the case (4), the case where the edge of A is at $x = X_f^1$. During the Möbius evolution, the t_1 -dependence of S_A is similar to the one in the cases (1)-(3). During the SSD evolution, that of S_A in case (4) is different from that in (1)-(3). In the SSD limit where $\theta \rightarrow \infty$, S_A monotonically grows with t_1 , and then it is, for large t_1 , approximated by

$$S_A \approx \frac{c}{6} \log(t_1) + \frac{c\pi L}{24\epsilon} + \frac{c}{6} \log \left[\frac{8\epsilon}{L} \left| \sin \left(\frac{\pi X_1}{L} \right) \right|^2 \right], \quad (3.16)$$

where the first term is the logarithmic function of t_1 , while the second term is the entanglement entropy of thermal entropy with 4ϵ for the half space. Thus, in case (4), S_A is

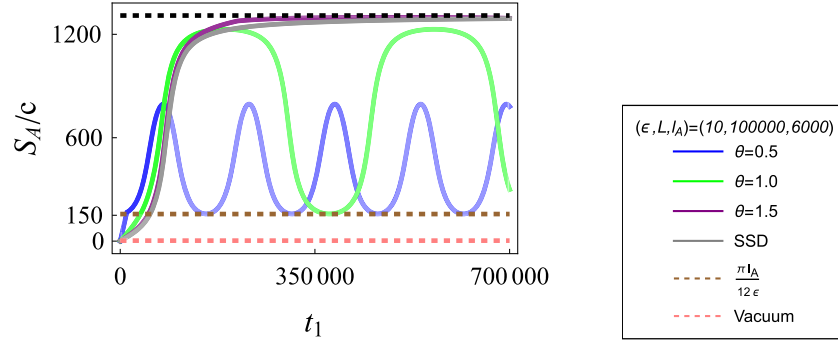


FIG. 5. The t_1 -dependence of S_A during the evolution induced by the Möbius and SSD Hamiltonians. In this figure, we take X_2 to be X_f^1 . The black dashed line illustrates the entanglement entropy for half of the total space of the thermal state with 4ϵ , the inverse temperature. The gray and pink dashed lines illustrate S_A of this thermal state and the vacuum state.

not asymptotically approximated by the vacuum entanglement entropy. In Fig. 5, we depict S_A as a function of t_1 .²

D. Cooling time

We close this section by defining the cooling time that describes how fast the subsystem evolves to the vacuum state during the SSD time evolution. In 2D holographic CFT, except for case (4), the entanglement entropy for the single intervals, A , is approximated by the vacuum one in the late time regime that is defined by

$$t \gg t_* = \frac{L}{4\pi} \sqrt{\frac{L}{\epsilon} \cdot \frac{\sin\left(\frac{\pi(X_1 - X_2)}{L}\right)}{\sin\left(\frac{\pi X_1}{L}\right) \sin\left(\frac{\pi X_2}{L}\right)}} \quad (3.17)$$

$$\underset{L \gg X_1 - X_2}{\approx} \frac{L}{4\pi} \sqrt{\frac{\pi l_A}{\epsilon \sin\left(\frac{\pi X_1}{L}\right) \sin\left(\frac{\pi X_2}{L}\right)}},$$

where l_A denotes the size of the subsystem, A . Thus, we call t_* the cooling time. In this late time regime, $t \gg t_*$, the quasiparticle picture does not work well because the entanglement entropy following this picture is smaller than $\mathcal{O}(1)$. This suggests that even during the SSD time evolution of 2D free fermion, t_* characterizes the time for the subsystem to cool down to the vacuum state.

Incidentally, this is also the timescale it takes for the quasiparticle Rényi entropy to decay to an $\mathcal{O}(1)$ value. For intervals that are located away from the origin X_f^1 so that $0 < X_2 < X_1 < L$, at late times, when $t_1 \gg L$, the Rényi entropy of the quasiparticles are approximately given by

²One may worry that the entanglement entropy of a finite-size subsystem grows forever with time. However, there is a timescale over which holographic calculations become unreliable. This scale is determined by the time when the EoW brane collides with the cutoff surface. In particular, it is given by a polynomial in L , not an exponent in L . For more details, see Sec. VA.

$$S_A^{(n)}(t) \approx \frac{n+1}{n} \frac{cL}{24\epsilon} \left(\frac{L}{2\pi t_1}\right)^2 \frac{\sin\left(\frac{\pi(X_1 - X_2)}{L}\right)}{\sin\left(\frac{\pi X_1}{L}\right) \sin\left(\frac{\pi X_2}{L}\right)}. \quad (3.18)$$

For a subsystem that is much smaller than the total system, the quasiparticle Rényi entropy becomes $\mathcal{O}(1)$ when $t \sim t_*$ as defined in (3.17).

IV. THE TIME EVOLUTION OF MUTUAL INFORMATION IN 2D CFTS

Now, we consider the time dependence of mutual information during the SSD/Möbius evolution to see if the nonlocal correlation measured by the mutual information is also asymptotically approximated by that of the vacuum state. Divide the system into the subsystems, A and B , and $\overline{A \cup B}$, the complement to the union of A and B , and then define the mutual information as the linear combination of entanglement entropies,

$$I_{A,B} = S_A + S_B - S_{A \cup B}, \quad (4.1)$$

where $S_{\mathcal{V}=A,B,A \cup B}$ denotes the entanglement entropies for the reduced density matrix associated with $\mathcal{V} = A, B, A \cup B$, respectively. Let X_1 and X_2 denote the edges of A , and let Y_1 and Y_2 denote the edges of B . Here, we assume that $L > Y_1 > Y_2 > X_1 > X_2 > 0$ or $L > X_1 > Y_1 > Y_2 > X_2 > 0$, and A does not overlap with B . In this case, only the nonuniversal pieces of $S_{\mathcal{V}}$ contribute to the mutual information because the universal pieces cancel out with each other.

A. Time dependence of $I_{A,B}$ in 2D free fermion

Consider the mutual information of the boundary state under these inhomogeneous quenches. The quasiparticle picture describes the second Rényi mutual information of the free Dirac CFT well as seen in Fig. 6. Just as for the second Rényi entropy, the second Rényi mutual information does not depend on the boundary condition. The mutual information also shows the periodicity of $L \cosh 2\theta$

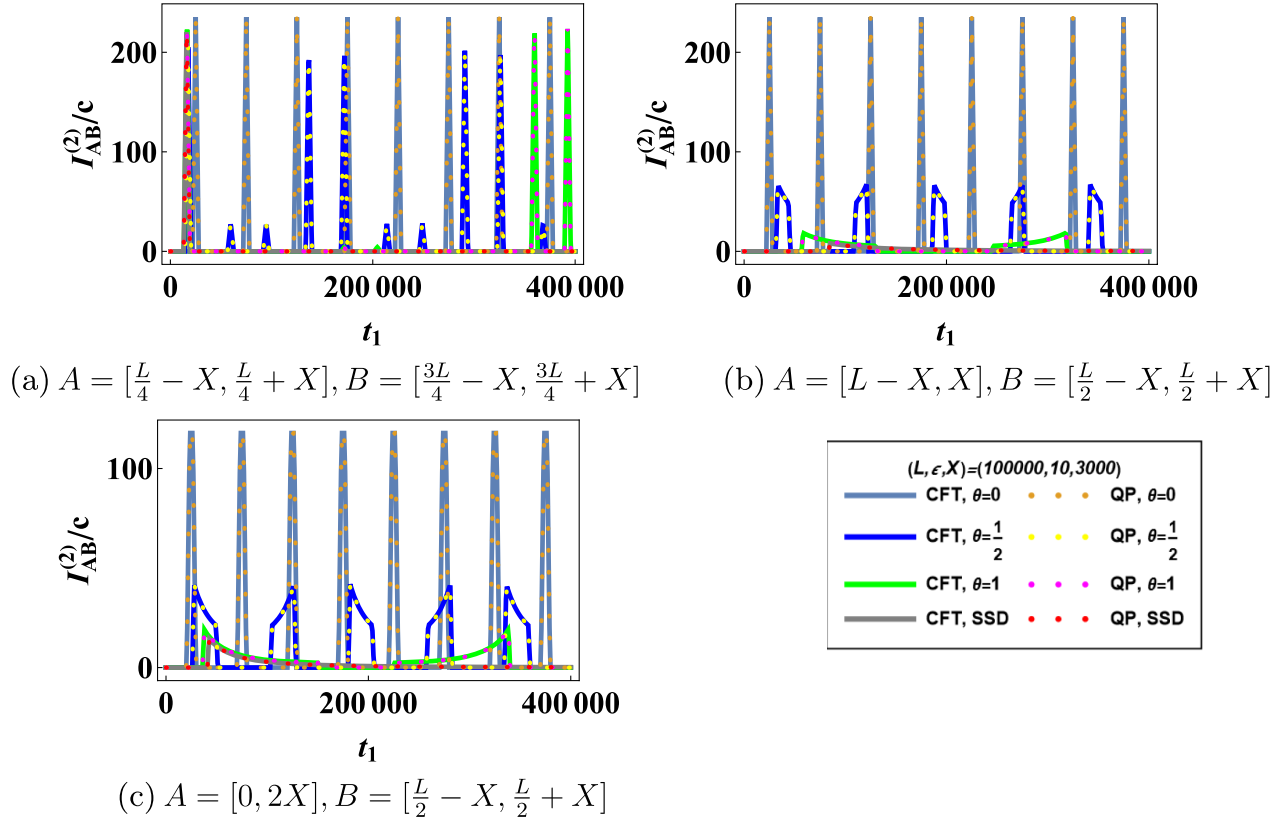


FIG. 6. Plots of the second Rényi mutual information for the free Dirac fermion as well as the quasiparticles for different placements of the subsystems of equal size $2X$. The total system size is fixed at $L = 100000$ while the regulator is set at $\epsilon = 10$. The subsystems are of size $2X$ with $X = 3000$. The continuous curves correspond to the CFT result while the dashed plots are the quasiparticle plots.

which goes to infinity in the SSD limit. For the setups shown in Fig. 6, the late time second Rényi mutual information of the free fermion boundary states after the SSD quench is given by the second Rényi mutual information for the vacuum state which is similar to the SSD quench of the spatially uniform thermal state [32].

When both subsystems are symmetrically placed away from the fixed point X_1^f as seen in the first plot [a], the uniform quench produces nonzero mutual information when the Bell pairs that are initially nearly equidistant from both subsystems enter these subsystems. As these quasiparticles and their partners make their way around the spatial circle, they pass through both subsystems giving rise to two peaks in the first period. The quasiparticles that begin at around $L/2$ and X_1^f reach both subsystems at about the same time which is no longer the case for Möbius quenches where the Bell pairs that begin at $L/2$ reach the subsystems earlier than those that begin near X_1^f , leading to a small second peak. The members of the quasiparticle pairs that begin near X_1^f then go on to enter their second subsystem, leading to a third small peak. Finally, when the members of the quasiparticles that begin near $L/2$ enter their second subsystem, we see a fourth peak in the first period. In the SSD limit, we only observe a single peak

since the quasiparticles are not able to go past the fixed point X_1^f . For both Möbius and SSD quenches, as the deformation parameter θ is increased, the speed of the quasiparticles near $L/2$ is greater so the first peak occurs earlier. The mutual information for the other two setups has peaks that are less symmetric but are nevertheless well-described by the quasiparticle picture.

B. Time dependence of $I_{A,B}$ in 2D holographic CFT

Now, we focus on the nonuniversal piece of S_{AUB} in 2D holographic CFT. We begin by computing the nonuniversal piece of S_{AUB} in the Euclidean space. In AdS/CFT correspondence, S_{AUB} is determined by the minimal geodesic length [78,79]:

$$S_{AUB, \text{Nonuni}} \approx \frac{2c}{3} \log\left(\frac{4\epsilon}{\pi}\right) + \frac{c}{12} \text{Min}[\mathcal{L}_{AUB, \text{con}}, \mathcal{L}_{AUB, \text{dis}}], \quad (4.2)$$

where $\mathcal{L}_{AUB, \text{con}}$ is the length of geodesic ending at the EoW brane, while $\mathcal{L}_{AUB, \text{dis}}$ is that of geodesic connecting two points at the same Euclidean time slice.

These nonuniversal pieces, $\mathcal{L}_{AUB, \text{con}}$ and $\mathcal{L}_{AUB, \text{dis}}$, are given by

$$\mathcal{L}_{A \cup B, \text{con}} = 2 \times \left[\sum_{i=1,2} \log \left\{ \cos \left(\frac{\pi(w_{X_i}^{\text{New},\alpha} + \bar{w}_{X_i}^{\text{New},\alpha})}{4\epsilon} \right) \cos \left(\frac{\pi(w_{Y_i}^{\text{New},\alpha} + \bar{w}_{Y_i}^{\text{New},\alpha})}{4\epsilon} \right) \right\} \right]$$

$$\mathcal{L}_{A \cup B, \text{dis}} = \text{Min}[\mathcal{L}_{A;\text{dis},1} + \mathcal{L}_{B;\text{dis},1}, \mathcal{L}_{A;\text{dis},2} + \mathcal{L}_{B;\text{dis},2}], \quad (4.3)$$

where $\mathcal{L}_{A;\text{dis},i=1,2}$ and $\mathcal{L}_{B;\text{dis},i=1,2}$ are defined in Appendix D. After performing the analytic continuation, $\tau_1 = it_1$, the minimal geodesic length determines the time dependence of $I_{A,B}$. In the early time regime where the nonuniversal pieces of $S_{\mathcal{V}=A,B,A \cup B}$ are determined by $S_{\mathcal{V},\text{con}}$, $S_{A \cup B}$ cancels out with $S_A + S_B$. Consequently, in this early time-regime, $I_{A,B}$ is zero. For the late time-regime where the nonuniversal pieces of $S_{\mathcal{V}}$ are determined by $S_{\mathcal{V},\text{dis}}$, the time-evolution of $I_{A,B}$ is determined by

$$I_{A,B} \approx \sum_{\mathcal{V}=A,B} \text{Min}[S_{\mathcal{V};\text{dis},1}, S_{\mathcal{V};\text{dis},2}] - \frac{c}{12} \text{Min}[\mathcal{L}_{A \cup B, \text{con}}, \mathcal{L}_{A \cup B, \text{dis}}]. \quad (4.4)$$

For the large t_1 -regime in the SSD limit, $I_{A,B}$ asymptotically reduces to the mutual information for the vacuum state,

$$I_{A,B} \approx \begin{cases} \text{Max} \left[0, \frac{\epsilon}{3} \log \left\{ \frac{\sin \left[\frac{\pi(X_1 - X_2)}{L} \right] \sin \left[\frac{\pi(Y_1 - Y_2)}{L} \right]}{\sin \left[\frac{\pi(Y_1 - X_2)}{L} \right] \sin \left[\frac{\pi(Y_2 - X_1)}{L} \right]} \right\} \right] & \text{for } X_f^1 \notin A \\ \text{Max} \left[0, \frac{\epsilon}{3} \log \left\{ \frac{\sin \left[\frac{\pi(X_1 - X_2)}{L} \right] \sin \left[\frac{\pi(Y_1 - Y_2)}{L} \right]}{\sin \left[\frac{\pi(X_1 - Y_1)}{L} \right] \sin \left[\frac{\pi(Y_2 - X_2)}{L} \right]} \right\} \right] & \text{for } X_f^1 \in A \end{cases}. \quad (4.5)$$

When the endpoint of A or B is at $x = X_f^1$, $I_{A,B}$ is given by (4.5) for $X_f^1 \notin A$. In conclusion, when starting from a boundary state and time-evolving it with the SSD Hamiltonian, the entanglement entropy does not strictly approach that of the vacuum state. However, during the SSD time evolution, the mutual information may exactly approach that of the vacuum state. Furthermore, unless $x = X_f^1$ at the edges of A and B, the reduced density matrices for $\mathcal{V} = A, B, A \cup B$ are asymptotically approximated by the vacuum reduced density matrices

$$\rho_{\mathcal{V}=A,B,A \cup B}(t \gg 1) \approx \rho_{\mathcal{V}=A,B,A \cup B}^{\text{vacuum}}, \quad (4.6)$$

where $\rho_{\mathcal{V}}^{\text{vacuum}}$ is the vacuum reduced density matrices associated to \mathcal{V} .

V. GRAVITATIONAL DESCRIPTION AND CMERA INTERPRETATION

In this section, we will report on the gravity dual of the system considered in this paper. In addition, we will discuss an interpretation of the SSD time evolution operator as a

continuous multiscale entanglement normalization ansatz (cMERA) [80–82].

A. Gravitational description

The early-time dependence of S_A is determined by that of geodesic ending at the end of the world (EoW) brane. Here, we discuss the gravity dual of the deformed boundary state, especially the trajectory of the EoW brane. In the AdS/BCFT correspondence [75,76], the boundary effects we have discussed are explained by the insertion of the EoW brane into the bulk spacetime. The EoW brane is characterized by the brane tension T , which determines the boundary entropy in the calculation of the holographic entanglement entropy.

We consider three-dimensional Einstein gravity on asymptotically AdS space M with the dynamical brane located on Q ,

$$S = \frac{1}{16\pi G_N} \int_M \sqrt{-g}(R + 2) + \frac{1}{8\pi G_N} \int_{\partial M} \sqrt{-h}K + \frac{1}{8\pi G_N} \int_Q \sqrt{-h}(K - T), \quad (5.1)$$

where we fixed the AdS radius to be unity, and G_N is Newton's constant. On the one hand, we impose the Dirichlet boundary conditions on the metric at the asymptotic boundary ∂M . On the other hand, we impose the Neumann boundary condition on Q which is necessary to consider the dynamical brane. Note that we have already fixed the matter profile on Q , characterized by the constant brane tension T , so that the boundary conformal symmetry is preserved.

As a solution of Einstein's equation, we obtain the BTZ black hole metric

$$ds^2 = (r^2 - r_+^2)d\tau^2 + \frac{dr^2}{r^2 - r_+^2} + r^2 dx^2 \quad (5.2)$$

with the EoW brane, whose (Euclidean) trajectory is given by

$$r(\tau) = \frac{r_+}{\sqrt{1 - T^2}} \sqrt{T^2 \tan^2(r_+ \tau) + 1}, \quad (5.3)$$

where $-1 < T < 1$. Throughout this subsection, we assume the length of circumference is 2π . In the CFT part, we have discussed only the case $T = 0$, while here we

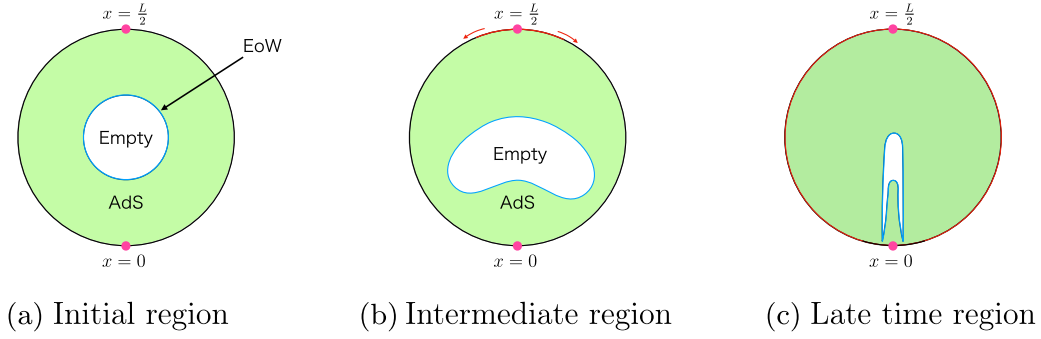


FIG. 7. A schematic view of motion of EoW brane under the SSD evolution ($\alpha = 0$) with nonpositive brane tension $T \leq 0$. In this picture, time flows from the left panel to the right panel. The reduced density matrix in the red region is approximated by that for the vacuum state. The size of the red region grows with time following the deformation of the EoW brane.

will discuss the more general value of T . For positive tension $T > 0$, the EoW brane is located on the other asymptotic boundary of a maximally extended solution. On the other hand, for negative tension $T < 0$, the EoW brane is outside of the horizon. In both cases, the brane eliminates the spacetime behind it, as the name suggests. In what follows, we mainly focus on the point of view of the boundary observer. Therefore, we shall discuss nonpositive tension brane.

Let us describe the trajectory of EoW brane on the deformed black hole geometry. To this end, we follow the prescription discussed in [32]. Namely, we rescale the radial coordinate r by the conformal factor and use the w^{New} coordinates discussed in Appendix A 2. After this replacement, we perform the analytic continuation to the Lorentzian time t_1 . Consequently, the t_1 -dependence of radial location is determined by

$$r(\tau) \rightarrow r'(t_1, x) = r(\tau_{\text{New}}(t_1, x)) \sqrt{\left(\frac{dw_x^{\text{New}, \alpha}}{dw_x}\right) \left(\frac{d\bar{w}_x^{\text{New}, \alpha}}{d\bar{w}_x}\right)}, \quad (5.4)$$

where $\tau_{\text{New}}(t_1, x) = (w_x^{\text{New}, \alpha} + \bar{w}_x^{\text{New}, \alpha})/2$. Note that since the new coordinates depend on both t_1 and x , the brane trajectory also acquires the spatial inhomogeneity. See Fig. 7 for a schematic picture of the motion of the EoW brane from the outside observer. In Figs. 8 and 9, we plot the spatial and time dependence of brane trajectories determined by (5.4) in SSD limit ($\alpha = 0$, see Fig. 8) and Möbius Hamiltonian ($\alpha = 1$, see Fig. 9) with small θ . It is worth noting that for sufficiently large θ , the time dependence reduces to the one in the SSD limit.

The existence of EoW brane becomes clear when we discuss holographic entanglement entropy with a large subsystem compared with the inverse temperature $\beta = 2\pi/r_+$ ($= 4\epsilon$). In this case, the holographic entanglement entropy is calculated from the phase where the minimal surfaces end on the EoW brane.

As a reference, we also plot the geodesic distance between the location of the EoW brane with negative tension and horizon as L_{bh} , although our true geometry ends at the EoW brane. See Fig. 10. These figures suggest that the size of the domain eliminated by the EoW brane comes to depend on the location. In particular, such regions are more likely to be eliminated in the early time.

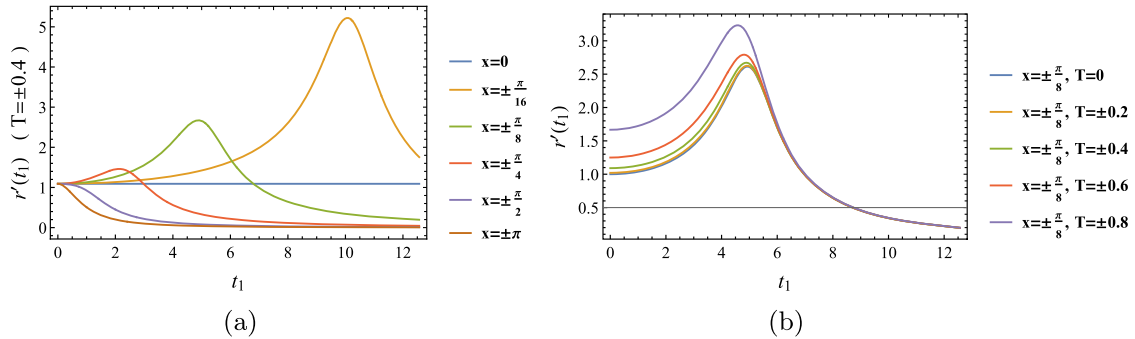


FIG. 8. (a) Time-dependence of brane trajectory in SSD limit with $T = \pm 0.4$. (b) Time-dependence of brane trajectory in SSD limit with $x = \pm \pi/8$. Here, we set $r_+ = 1$.

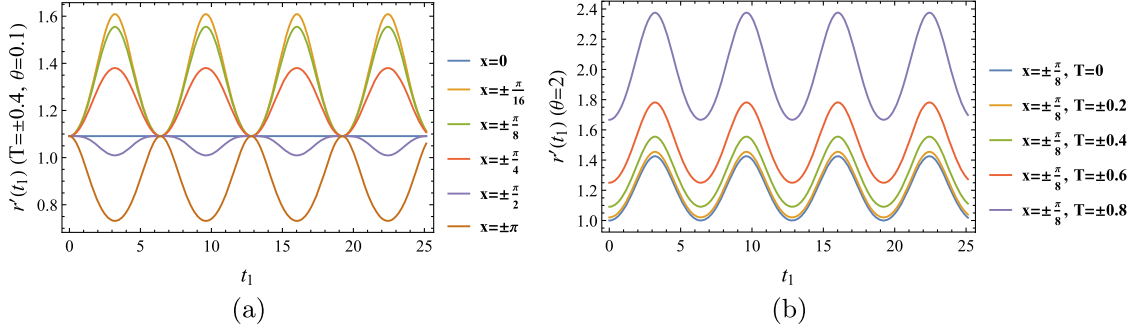


FIG. 9. (a) Time-dependence of brane trajectory with $\theta = 0.1$ and $T = \pm 0.4$. (b) Time-dependence of brane trajectory with $\theta = 0.1$ and $x = \pm\pi/8$. Here we set $r_+ = 1$.

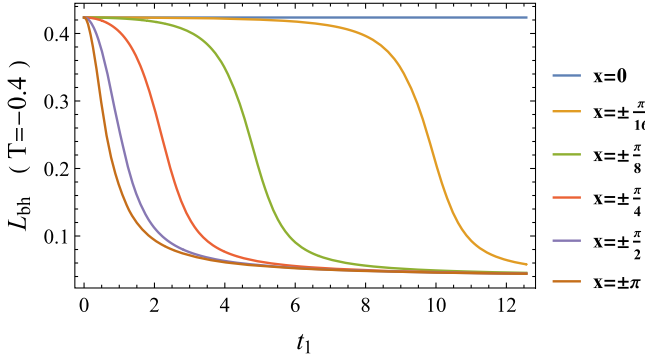


FIG. 10. Geodesic distance between EoW with negative tension ($T = -0.4$) and black hole horizon for the original geometry. Here we show the case of SSD limit.

1. Comments on cutoff surface

As we have seen so far, the EoW brane approaches the asymptotic boundary. At sufficiently late time, $t \gg L$, the location of the horizon's peak grows linearly in time [32],

$$r'_{\text{horizon}} = \frac{r_+ \sqrt{L^2 + \pi^2 t^2}}{L} \simeq \frac{\pi r_+ t}{L}. \quad (5.5)$$

This is also the case for the brane because the distance between the brane and horizon becomes a constant value at the late time.

On the other hand, we should introduce a cutoff surface on a certain radial scale $r' = r_\infty$ that determines the UV cutoff for the dual CFT. It means that the EoW will eventually collide with the cutoff surface at some time. We interpret this as the timescale on which the holographic calculation in Sec. III C 3 becomes unreliable.³ More concretely, we cannot

³If the cutoff surface is defined globally, as it is in much of the literature, this collision problem should occur in all holographic calculations. Nevertheless, for all holographic calculations except Sec. III C 3, any immediate problems do not occur as we have seen. This observation suggests that we have to define the cutoff surface locally around the entangling surface. Note that this is a natural prescription from the CFT side [83] and its gravity dual [84].

trust our calculation after $t \sim L/r_+ \epsilon_{\text{UV}}$. Here we introduced the cutoff length scale in the dual CFT ϵ_{UV} such that $r_\infty = 1/\epsilon_{\text{UV}}$.

B. cMERA interpretation

Here, we discuss an interpretation of the Möbius/SSD time evolution operator as a continuous multiscale entanglement normalization ansatz (cMERA).

1. A brief review of MERA and cMERA

In this section, we begin by reviewing the MERA shortly, and subsequently review the cMERA. The MERA is the scheme of the renormalization group in terms of a tensor network constructed of the two kinds of tensors [85–87]. This is suitable for the (numerical) computation in the discrete system at the critical point. The tensor network in the MERA has a discrete layered structure where we have the discrete energy scale direction perpendicular to the space-time direction. We label this discrete energy scale direction by u , and we assume that $u = 0, -1, \dots, -\infty$. On each layer at u , the tensor network is constructed of two types of tensors, called isometry and (dis-)entangler. Let \mathcal{L} and K denote the isometry and entangler. The isometry is a linear map where two nearest spins at u reduce to a single spin at $u - 1$. Since this resembles the coarse-graining or the scale transformation, the isometry is considered as these operations in MERA. If the dimension of Hilbert space at $u = 0$ is 2^L , where L is the system size, then the one at u is estimated with 2^{2^L} . The entangler is the unitary operator acting the two nearest spins at u . This tensor endows the state with short-range entanglement. We start from an unentangled state $|\Omega\rangle$ that is invariant under the scale transformation generator \mathcal{L} ,

$$\mathcal{L}|\Omega\rangle = 0, \quad (5.6)$$

and then nonunitarily evolve the system from $u = -\infty$ to $u = 0$ with the circuit constructed of the isometries and entanglers. We call $|\Omega\rangle$ the reference state, while we call the state at $u = 0$ the target state. We tune the parameters of

isometries and entanglers so that the target state is the state of interest.

Let us begin the review of cMERA. The cMERA is designed to be suitable for the (numerical) computation in the quantum field theories at the critical point. Define the state at $u = -\infty$ as

$$\mathcal{L}|\Omega\rangle = 0, \quad (5.7)$$

where \mathcal{L} is the scale transformation generator as in the MERA. However, in the cMERA, the isometry is replaced with a unitary operator. Since the isometry and entangler preserve the dimension of Hilbert space at each step u , the tensor network in the cMERA is a unitary evolution operator. We assume that the energy scale is labeled by the continuous parameter u . Consequently, under the cMERA, the system unitarily evolves with the unitary evolution operator to the target state,

$$|\Psi(0)\rangle = U(0, -\infty)|\Omega\rangle = \mathcal{P}e^{-i\int_{-\infty}^0 du(K(u)+\mathcal{L})}|\Omega\rangle, \quad (5.8)$$

where \mathcal{P} is defined as the path-ordering operator arranging the operators in order of increasing u from right to left. The symbols, $K(u)$ and \mathcal{L} , are defined as the integrals of entangler and isometry densities along the spatial directions, respectively.

Furthermore, define the state and entangler in the interaction picture, $|\Psi_I(u)\rangle$ and $\hat{K}(u)$, as

$$|\Psi_I(u)\rangle = e^{i\mathcal{L}u}|\Psi(u)\rangle, \quad \hat{K}(u) = e^{i\mathcal{L}u}K(u)e^{-i\mathcal{L}u}. \quad (5.9)$$

Consequently, the target state in the interaction picture is given by

$$|\Psi_I(0)\rangle = |\Psi(0)\rangle = \mathcal{P}e^{-i\int_{-\infty}^0 du\hat{K}(u)}|\Omega\rangle. \quad (5.10)$$

Thus, $|\Psi_I(0)\rangle$ does not depend on the definition of \mathcal{L} .

2. A cMERA interpretation on the Möbius/SSD time evolution

Now, we turn to the quenches induced by Möbius/SSD Hamiltonians, and discuss the interpretation for these quenches as the cMERA. As in [68], we employ the boundary state with the proper regularization as the reference state,

$$|\Omega\rangle = e^{-\epsilon H}|\Psi_0\rangle, \quad (5.11)$$

where the Hamiltonian H is defined as $H = (2\pi(L_0 + \bar{L}_0))/L - (c\pi)/6L$, where L_n and \bar{L}_n are chiral and antichiral Virasoro generators. In addition to them, the boundary state is defined as

$$(L_n - \bar{L}_n)|\Psi_0\rangle = 0. \quad (5.12)$$

In this paper, unlike the common procedure in cMERA, we define the operator that keeps the reference state invariant as \mathcal{L} . We utilize the spin operator $(2\pi(L_0 - \bar{L}_0))/L$ as \mathcal{L} .

Subsequently, we consider t_1 during the time evolution as the energy scale u in the tensor network as in [88,89]. We start from the boundary state $|\Omega\rangle$ at $t_1 = -U_{\text{IR}}$ and evolve the system up to $t_1 = 0$. This is equivalent to the time evolution from $t_1 = 0$ to $t = U_{\text{IR}}$ as considered in Secs. III A and III C. The depth of the time evolution and tensor network in cMERA is determined by U_{IR} .

Möbius/SSD time evolution We begin by considering the quantum quench induced by the Möbius Hamiltonian. Divide the Möbius Hamiltonian into the entangler $K(\theta)$ and the isometry \mathcal{L} ,

$$\begin{aligned} H_{\text{Möbius}} &= K(\theta) + \mathcal{L}, \\ K(\theta) &= \frac{2\pi}{L} \left[L_0 + \bar{L}_0 \right. \\ &\quad \left. - \frac{\tanh 2\theta}{2} (L_1 + L_{-1} + \bar{L}_1 + \bar{L}_{-1}) - (L_0 - \bar{L}_0) \right], \\ \mathcal{L} &= \frac{2\pi}{L} (L_0 - \bar{L}_0), \end{aligned} \quad (5.13)$$

where we express $H_{\text{Möbius}}$, $K(\theta)$, and \mathcal{L} in terms of Virasoro generators. In the interaction picture, $|\Psi_I(0)\rangle$ is given by

$$|\Psi_I(0)\rangle = |\Psi(0)\rangle = \mathcal{T}e^{-i\int_{-U_{\text{IR}}}^0 dt_1 \hat{K}(\theta, t_1)}|\Omega\rangle, \quad (5.14)$$

where \mathcal{T} is defined as the time-ordering operator arranging the operators in order of increasing t_1 from right to left, and $\hat{K}(\theta, t_1)$ is defined by $\hat{K}(\theta, t_1) = e^{i\mathcal{L}t_1}K(\theta)e^{-i\mathcal{L}t_1}$. Thus, $|\Psi_I(0)\rangle$ does not depend on the definition of \mathcal{L} . The entangler in the interaction picture is explicitly given by

$$\begin{aligned} \hat{K}(\theta, t_1) &= H_0 - \mathcal{L} + i \sin\left(\frac{2\pi t_1}{L}\right)\tilde{H}(\theta) \\ &\quad + \cos\left(\frac{2\pi t_1}{L}\right)(H_{\text{Möbius}} - H_0) \end{aligned} \quad (5.15)$$

where H_0 and $\tilde{H}(\theta)$ are defined by

$$\begin{aligned} H_0 &= \frac{2\pi}{L} (L_0 + \bar{L}_0), \\ \tilde{H}(\theta) &= \frac{\tanh 2\theta}{2} \left(\frac{2\pi}{L}\right) (L_1 - L_{-1} - \bar{L}_1 + \bar{L}_{-1}). \end{aligned} \quad (5.16)$$

This entangler in the interaction picture possesses the periodicity with t_1 ,

$$\hat{K}(\theta, t_1 + L) = \hat{K}(\theta, t_1). \quad (5.17)$$

This period is independent of the parameter θ . In the SSD limit where $\theta \rightarrow \infty$, $\hat{K}(\theta)$ reduces to \tilde{K} ,

$$\tilde{K} = \frac{2\pi}{L} \left[L_0 + \bar{L}_0 - \frac{1}{2}(L_1 + L_{-1} + \bar{L}_1 + \bar{L}_{-1}) - (L_0 - \bar{L}_0) \right]. \quad (5.18)$$

Consequently, the entangler in the interaction picture is given by replacing $H_{\text{Möbius}}$ in (5.15) with H_{SSD} .

Expression in terms of spin variables We will rewrite the entanglers in the interaction picture in terms of spin variables that suit experimental research.

As explained in [90], these Virasoro generators can be realized in certain spin chains with N sites governed by a Hamiltonian that can be expressed as a sum of Temperley-Lieb generators e_i ,

$$H = - \sum_{i=1}^{N-1} e_i. \quad (5.19)$$

The generators e_i satisfy the Temperley-Lieb algebra whose exact form is not necessary for our purposes. For a spin- $\frac{1}{2}$ chain, one possible representation of this algebra is given by

$$e_i = \frac{q + q^{-1}}{4} - \frac{1}{2} \left(X_i X_{i+1} + Y_i Y_{i+1} + \frac{q + q^{-1}}{2} Z_i Z_{i+1} \right) - \frac{q - q^{-1}}{4} (Z_i - Z_{i+1}), \quad (5.20)$$

where X_i , Y_i , and Z_i are Pauli matrices acting on site i and q is an arbitrary complex parameter although the physically interesting cases are obtained when q is a root of unity. With this representation of the Temperley-Lieb algebra, the Hamiltonian (5.19) is, up to an inconsequential constant, the XXZ Hamiltonian that contains some additional boundary terms

$$H = \frac{1}{2} \sum_{i=1}^{N-1} \left(X_i X_{i+1} + Y_i Y_{i+1} + \frac{q + q^{-1}}{2} Z_i Z_{i+1} \right) + \frac{q - q^{-1}}{4} (Z_1 - Z_N). \quad (5.21)$$

The standard Heisenberg spin chain can be obtained by simply setting $q = 1$. It is conjectured, with substantial evidence, that the lattice operators

$$L_n^{(N)} = \frac{N}{\pi} \left[-\frac{1}{v_F} \sum_{k=1}^{N-1} (e_k - e_\infty) \cos\left(\frac{nk\pi}{N}\right) + \frac{1}{v_F^2} \sum_{k=1}^{N-2} [e_k, e_{k+1}] \sin\left(\frac{nk\pi}{N}\right) \right] + \frac{c}{24} \delta_{n,0} \quad (5.22)$$

approaches the Virasoro generators L_n in the $N \rightarrow \infty$ continuum limit. Here, $v_F = \frac{\pi \sin \gamma}{\gamma}$ is the Fermi velocity and is determined by the q parameter via $2 \cos \gamma = q + q^{-1}$. For treatments of the Ising model and the XX spin chain, see Refs. [91] and [92] respectively.

VI. DISCUSSION AND FUTURE DIRECTIONS

We will discuss the relation between the gravity dual in the Heisenberg picture and the renormalization group, and comment on future directions.

A. Renormalization group and SSD evolution

In Sec. VA, we discussed the gravity dual in Schrödinger picture. In this picture, the EoW brane moves and is deformed during the Möbius/SSD time evolution. We can instead consider the gravity dual in the Heisenberg picture. In this picture, the location of EoW is pinned at the horizon of the BTZ black hole, while the location of the surface (UV surface) where CFT lives moves and is deformed in time. Let r_{UV} denote the radial location of this UV surface at $t_1 = 0$. The trajectory of r_{UV} during the Möbius/SSD time evolution is determined by

$$r_{\text{UV}}^{\text{BTZ}}(x, t_1) = \frac{r_{\text{UV}}}{\sqrt{\left(\frac{dw_x^{\text{New}}}{dw_x} \frac{d\bar{w}_x^{\text{New}}}{d\bar{w}_x} \right)}}. \quad (6.1)$$

Thus, the location of the UV surface depends on (x, t_1) .

In the AdS/CFT correspondence, the radial direction in the gravity dual is considered as the energy scale in the 2D CFT. In the coordinate considered in this paper, the larger r becomes, the larger the energy scale becomes. The spatial and temporal dependence of the r_{UV} suggests that the energy scale in 2D CFT depends on (x, t_1) . Except for the case discussed in Sec. III C 3, during SSD time evolution, S_A is eventually approximated by the vacuum entanglement entropy. This suggests that for the large t_1 , the location of the UV surface is further from the EoW than at $t_1 = 0$. In other words, in the large time regime, the energy scale is larger than the initial one. The location of the UV surface near $x = X_f^2$ gets further from the EoW faster. We can see from the spatial and time dependence of the UV surface that the reverse of SSD time evolution considered in this paper may be used as the renormalization group where the energy scale depends on the spatial location.

B. Future direction

We close this section with comments on the entanglement entropy for the large time regime. In this paper and [32], we propose the quasiparticle picture, an effective picture, describing the time dependence of entanglement entropy at $\mathcal{O}(\frac{1}{\epsilon})$. However, this does not describe the late-time entanglement entropy, the vacuum entanglement

entropy, because the vacuum one is at $\mathcal{O}(1)$. The findings in the inhomogeneous quench show that inhomogeneous evolution may endow the states with two types of entanglement structure: One of them is a dynamical entanglement structure that can be described by the propagation of quasiparticles, while the other is a static entanglement structure that remains after quasiparticles pass away [93]. Studying the static entanglement structure may lead to a deeper understanding of entanglement dynamics. We leave this as a future problem.

ACKNOWLEDGMENTS

We thank useful discussions with Shinsei Ryu. Especially, his suggestion of a relationship between SSDs and cMERA is illuminating for us. M. N. is supported by funds from the University of Chinese Academy of Sciences (UCAS), funds from the Kavli Institute for Theoretical Sciences (KITS). K. T. is supported by JSPS KAKENHI Grant No. 21K13920 and MEXT KAKENHI Grant No. 22H05265. M. T. is supported by an appointment to the YST Program at the APCTP through the Science and Technology Promotion Fund and Lottery Fund of the Korean Government, as well as the Korean Local Governments—Gyeongsangbuk-do Province and Pohang City.

APPENDIX A: THE LOCATION OF EVOLVED OPERATORS

The time evolution of local operator coordinates under Möbius/SSD evolution is explained in [57]. In order to keep this paper self-contained, we shall summarize the details here.

1. Operator trajectory

In order to derive the transformation of the primary operator under Euclidean time evolution, let us begin by expressing the Möbius Hamiltonian $H_{\text{Möbius}}$ in terms of the complex coordinates (w, \bar{w}) ,

$$H_{\text{Möbius}} = \frac{1}{2i\pi} \oint dw \left[T(w) - \frac{\tanh 2\theta}{2} (e^{\frac{2\pi w}{L}} + e^{-\frac{2\pi w}{L}}) T(w) \right] + \frac{1}{2i\pi} \oint d\bar{w} \left[\bar{T}(\bar{w}) - \frac{\tanh 2\theta}{2} (e^{\frac{2\pi \bar{w}}{L}} + e^{-\frac{2\pi \bar{w}}{L}}) \bar{T}(\bar{w}) \right]. \quad (\text{A1})$$

Under a conformal transformation from (w, \bar{w}) to (z, \bar{z}) , this Hamiltonian is expressed as

$$H_{\text{Möbius}} = \left(\frac{2\pi}{L} \right) \times \frac{1}{2i\pi} \oint dz \left[zT(z) - \frac{\tanh 2\theta}{2} (z^2 + 1)T(z) \right] + \left(\frac{2\pi}{L} \right) \times \frac{1}{2i\pi} \oint d\bar{z} \left[\bar{z}\bar{T}(\bar{z}) - \frac{\tanh 2\theta}{2} (\bar{z}^2 + 1)\bar{T}(\bar{z}) \right] - \frac{c}{12} \times \left(\frac{2\pi}{L} \right). \quad (\text{A2})$$

Next, perform a second conformal transformation from (z, \bar{z}) to $(\tilde{z}, \bar{\tilde{z}}) = \left(\frac{-\cosh \theta z + \sinh \theta}{-\cosh \theta + \sinh \theta z}, \frac{-\cosh \theta \bar{z} + \sinh \theta}{-\cosh \theta + \sinh \theta \bar{z}} \right)$. In these new coordinates, the Möbius Hamiltonian takes the simple form,

$$H_{\text{Möbius}} = \left(\frac{2\pi}{L} \right) \times \frac{1}{2i\pi} \left[\oint d\tilde{z} \tilde{z} T(\tilde{z}) + \oint d\bar{\tilde{z}} \bar{\tilde{z}} \bar{T}(\bar{\tilde{z}}) \right] - \frac{c}{12} \times \left(\frac{2\pi}{L} \right) = \left(\frac{2\pi}{L_{\text{eff}}} \right) \times \left[L_0^{\tilde{z}} + L_0^{\bar{\tilde{z}}} - \frac{c}{12} \right], \quad (\text{A3})$$

where the Virasoro generators in the $(\tilde{z}, \bar{\tilde{z}})$ coordinates are written in terms of the stress energy tensor as

$$L_n^{\tilde{z}} = \frac{1}{2i\pi} \oint d\tilde{z} \tilde{z}^{n+1} T(\tilde{z}), \quad \bar{L}_n^{\bar{\tilde{z}}} = \frac{1}{2i\pi} \oint d\bar{\tilde{z}} \bar{\tilde{z}}^{n+1} \bar{T}(\bar{\tilde{z}}). \quad (\text{A4})$$

In the $(\tilde{z}, \bar{\tilde{z}})$ coordinates, the Möbius Hamiltonian is the usual uniform Hamiltonian which is the generator of dilatations on the complex plane, so a primary operator in the $(\tilde{z}, \bar{\tilde{z}})$ coordinates transforms in a simple manner under the Möbius Hamiltonian as

$$\mathcal{O}_H(\tilde{z}, \bar{\tilde{z}}, a) := e^{aH_{\text{Möbius}}} \mathcal{O}(\tilde{z}, \bar{\tilde{z}}) e^{-aH_{\text{Möbius}}} = \lambda_{\text{eff}}^{2h_{\mathcal{O}}} \mathcal{O}(\lambda_{\text{eff}} \tilde{z}, \lambda_{\text{eff}} \bar{\tilde{z}}), \quad (\text{A5})$$

where the scaling factor λ_{eff} is related to θ as well as a by

$$\lambda_{\text{eff}} := e^{\frac{2\pi a}{L \cosh 2\theta}}. \quad (\text{A6})$$

Define a final set of complex coordinates $(w_{a,\text{Möbius}}^{\text{New}}, \bar{w}_{a,\text{Möbius}}^{\text{New}})$ as

$$\left(e^{\frac{2\pi w_{a,\text{Möbius}}^{\text{New}}}{L}}, e^{\frac{2\pi \bar{w}_{a,\text{Möbius}}^{\text{New}}}{L}} \right) := (\lambda_{\text{eff}} \tilde{z}, \lambda_{\text{eff}} \bar{\tilde{z}}). \quad (\text{A7})$$

Putting it all together, we arrive at the conformal transformation for a primary operator under a Möbius evolution

$$e^{aH_{\text{Möbius}}} \mathcal{O}(w, \bar{w}) e^{-aH_{\text{Möbius}}} = \left| \frac{dw_{a,\text{Möbius}}^{\text{New}}}{dw} \right|^{2h_{\mathcal{O}}} \mathcal{O}(w_{a,\text{Möbius}}^{\text{New}}, \bar{w}_{a,\text{Möbius}}^{\text{New}}) \quad (\text{A8})$$

This is one of the key identities used in this paper. The conformal transformation of primary operators under an SSD evolution is obtained by taking the $\theta \rightarrow \infty$ limit of the conformal transformation produced by the corresponding Möbius evolution. Let us also check if the local primary operators obey the Ward-Takahashi identity. The Schrödinger equation of a local primary operator with a time coordinate a in the $(\tilde{z}, \bar{\tilde{z}})$ complex coordinates is

$$\frac{d\mathcal{O}_{\text{H}}(\tilde{z}, \bar{\tilde{z}}, a)}{da} = \frac{2\pi}{L_{\text{eff}}} [2h_{\mathcal{O}}\mathcal{O}_{\text{H}}(\tilde{z}, \bar{\tilde{z}}, a) + \tilde{z}\partial_{\tilde{z}}\mathcal{O}_{\text{H}}(\tilde{z}, \bar{\tilde{z}}, a) + \bar{\tilde{z}}\partial_{\bar{\tilde{z}}}\mathcal{O}_{\text{H}}(\tilde{z}, \bar{\tilde{z}}, a)]. \quad (\text{A9})$$

This is also the transformation of $\mathcal{O}_{\text{H}}(\tilde{z}, \bar{\tilde{z}}, a)$ generated by the Möbius Hamiltonian

$$\begin{aligned} \frac{d\mathcal{O}_{\text{H}}(\tilde{z}, \bar{\tilde{z}}, a)}{da} &= [H_{\text{Möbius}}, \mathcal{O}_{\text{H}}(\tilde{z}, \bar{\tilde{z}}, a)] \\ &= \left[\left(\frac{2\pi}{L_{\text{eff}}} \right) \cdot \left[L_0^{\tilde{z}} + L_0^{\bar{\tilde{z}}} - \frac{c}{12} \right], \mathcal{O}_{\text{H}}(\tilde{z}, \bar{\tilde{z}}, a) \right]. \end{aligned} \quad (\text{A10})$$

Expanding the Möbius Hamiltonian in terms of Virasoro generators in the (z, \bar{z}) coordinates,

$$H_{\text{Möbius}} = \frac{2\pi}{L} \left[L_0^z + \bar{L}_0^{\bar{z}} - \frac{\tanh 2\theta}{2} (L_1^z + L_{-1}^z + \bar{L}_1^{\bar{z}} + \bar{L}_{-1}^{\bar{z}}) \right], \quad (\text{A11})$$

and substituting this into the Schrödinger equation in the complex coordinates, (z, \bar{z}) , we obtain

$$\begin{aligned} \frac{d\mathcal{O}_{\text{H}}(z, \bar{z}, a)}{da} &= [H_{\text{Möbius}}, \mathcal{O}_{\text{H}}(z, \bar{z}, a)] = \frac{2\pi}{L} \left[L_0^z + \bar{L}_0^{\bar{z}} - \frac{\tanh 2\theta}{2} (L_1^z + L_{-1}^z + \bar{L}_1^{\bar{z}} + \bar{L}_{-1}^{\bar{z}}), \mathcal{O}_{\text{H}}(z, \bar{z}, a) \right] \\ &= \frac{2\pi}{L_{\text{eff}}} \left[h_{\mathcal{O}}(\cosh 2\theta - z \sinh 2\theta) \mathcal{O}_{\text{H}}(z, \bar{z}, a) + \left(z \cosh 2\theta - \frac{\sinh 2\theta}{2} (1 + z^2) \right) \partial_z \mathcal{O}_{\text{H}}(z, \bar{z}, a) \right] \\ &\quad + \frac{2\pi}{L_{\text{eff}}} \left[h_{\mathcal{O}}(\cosh 2\theta - \bar{z} \sinh 2\theta) \mathcal{O}_{\text{H}}(z, \bar{z}, a) + \left(z \cosh 2\theta - \frac{\sinh 2\theta}{2} (1 + \bar{z}^2) \right) \partial_{\bar{z}} \mathcal{O}_{\text{H}}(z, \bar{z}, a) \right]. \end{aligned} \quad (\text{A12})$$

This equation (A12) can also be obtained from (A10) by performing a change of coordinates from $(\tilde{z}, \bar{\tilde{z}})$ to (z, \bar{z}) . Hence, both equations (A12) and (A10) are consistent with each other.

2. Before the analytic continuation

In terms of τ_1 and x , $w_x^{\text{New},\alpha}$ and $\bar{w}_x^{\text{New},\alpha}$ are given by

$$\begin{aligned} w_x^{\text{New},\alpha} + \epsilon &= \tau_{x,\tau_1,\alpha} + i \frac{L\varphi_{x,\tau_1,\alpha}}{2\pi}, \quad \bar{w}_x^{\text{New},\alpha} + \epsilon = \tau_{x,\tau_1,\alpha} + i \frac{L\bar{\varphi}_{x,\tau_1,\alpha}}{2\pi}, \\ \tau_{x,\tau_1,0} &= \epsilon - \log \left[2(\pi\tau_1)^2 \left(1 - \cos\left(\frac{2\pi x}{L}\right) \right) + L^2 - 2\pi\tau_1 L \left(1 - \cos\left(\frac{2\pi x}{L}\right) \right) \right] + \frac{L}{2\pi} \log r_{x,\tau_1,0}, \\ r_{x,\tau_1,0} &= \sqrt{\left(2(\pi\tau_1)^2 \left(1 - \cos\left(\frac{2\pi x}{L}\right) \right) + L^2 \cos\left(\frac{2\pi x}{L}\right) \right)^2 + \left(L^2 \sin\left(\frac{2\pi x}{L}\right) \right)^2}, \\ \cos \varphi_{x,\tau_1,0} &= \cos \bar{\varphi}_{x,\tau_1,0} = \frac{2(\pi\tau_1)^2 (1 - \cos(\frac{2\pi x}{L})) + L^2 \cos(\frac{2\pi x}{L})}{r_{x,\tau_1,0}}, \\ \sin \varphi_{x,\tau_1,0} &= -\sin \bar{\varphi}_{x,\tau_1,0} = \frac{L^2 \sin(\frac{2\pi x}{L})}{r_{x,\tau_1,0}}, \\ \tau_{x,\tau_1,1} &= \epsilon + \frac{L}{2\pi} \log r_{x,\tau_1,1} - \log \left[(1 - \lambda_1)^2 \sinh^2(2\theta) + ((\lambda_1 - 1) \cosh 2\theta - (\lambda_1 + 1))^2 \right. \\ &\quad \left. + 2(1 - \lambda_1) \sinh(2\theta) ((\lambda_1 - 1) \cosh 2\theta - (\lambda_1 + 1)) \cos\left(\frac{2\pi x}{L}\right) \right] \end{aligned}$$

$$\begin{aligned}
r_{x,\tau_1,1} &= \sqrt{\left[(1-\lambda_1)^2 \sinh 4\theta + -(1-\lambda_1)^2 \cosh 4\theta + (1+\lambda_1)^2 \cos\left(\frac{2\pi x}{L}\right) \right]^2 + 16\lambda_1^2 \sin^2\left(\frac{2\pi x}{L}\right)}, \\
\cos \varphi_{x,\tau_1,1} &= \cos \bar{\varphi}_{x,\tau_1,1} = \frac{(1-\lambda_1)^2 \sinh 4\theta + -(1-\lambda_1)^2 \cosh 4\theta + (1+\lambda_1)^2 \cos\left(\frac{2\pi x}{L}\right)}{r_{x,\tau_1,1}}, \\
\sin \varphi_{x,\tau_1,1} &= -\sin \bar{\varphi}_{x,\tau_1,1} = \frac{4\lambda_1 \sin\left(\frac{2\pi x}{L}\right)}{r_{x,\tau_1,1}}, \lambda_1 = e^{\frac{2\pi\tau_1}{L \cosh 2\theta}},
\end{aligned} \tag{A13}$$

Thus, the location in Euclidean time direction of twist and antitwist operator is $\tau = \tau_{x,\tau_1,\alpha}$.

a. Analytic continuation

We finally perform the analytic continuation to the real time:

$$\tau_1 = it_1. \tag{A14}$$

APPENDIX B: ENTANGLEMENT ENTROPY FOR THE SINGLE INTERVAL IN 2D MASSLESS FREE FERMION AND HOLOGRAPHIC CFTs

In this paper, we will describe the details of the computation of the entanglement entropy for the single interval in 2D massless free fermion and holographic CFTs.

1. Entanglement entropy for the single interval in 2D massless free fermion

The entanglement entropy of the free Dirac fermion after an inhomogeneous quench of a boundary state can be

computed using bosonization similar to that in [94,95] but with the time evolution Hamiltonian replaced with the Möbius Hamiltonian. The n th moment of the reduced density matrix for a single interval is

$$\begin{aligned}
&\langle \Psi_0 | e^{-2\epsilon H} \mathcal{T}_n(w_i, \bar{w}_i) \bar{\mathcal{T}}_n(w_j, \bar{w}_j) | \Psi_0 \rangle_{\text{Cylinder}} \\
&= \left(\frac{2\pi}{L}\right)^{4h_n} \prod_{a=-\frac{n-1}{2}}^{\frac{n-1}{2}} \frac{\langle \Psi_0 | e^{-2\epsilon H} \mathcal{T}^{(a)}(y_i, \bar{y}_i) \mathcal{T}^{(-a)}(y_j, \bar{y}_j) | \Psi_0 \rangle}{\langle \Psi_0 | e^{-2\epsilon H} | \Psi_0 \rangle}
\end{aligned} \tag{B1}$$

where $|\Psi_0\rangle$ is the boundary state that lives on the ends of the cylinder and there is a conformal factor that comes from rescaling the correlation function so that the spatial coordinate has a periodicity of L instead of 2π . Let $y = \tau - i\sigma$ where $0 \leq \tau \leq 2\epsilon$ and $0 \leq \sigma \leq 2\pi$ be the holomorphic coordinate on this rescaled cylinder. Applying the bosonization dictionary, the twist operators can be written as twisted vertex operators that depend on the boundary condition,

$$\mathcal{T}^{(a)}(y, \bar{y}) = \begin{cases} \mathcal{T}_1^{(a)}(y, \bar{y}) = V_{\left(\frac{a}{n}, -\frac{a}{n}\right)}(y, \bar{y}) = e^{i\frac{a}{n}(X_L(y) - X_R(\bar{y}))} & \text{Neumann B.C.} \\ \mathcal{T}_2^{(a)}(y, \bar{y}) = V_{\left(\frac{a}{n}, \frac{a}{n}\right)}(y, \bar{y}) = e^{i\frac{a}{n}(X_L(y) + X_R(\bar{y}))} & \text{Dirichlet B.C.} \end{cases}. \tag{B2}$$

The correlation function of vertex operators in the boundary state can be computed by writing the vertex operators and the boundary state in terms of the bosonic modes and by repeatedly applying the bosonic commutation and the Baker-Campbell-Hausdorff relations [94]. The denominator is the partition function for the finite cylinder with boundary states $|\Psi_0\rangle$ on both ends as is given by

$$\langle \Psi_0 | e^{-2\epsilon H} | \Psi_0 \rangle = \begin{cases} \frac{\theta_3(0|\frac{i4\epsilon}{L}) + \theta_2(0|\frac{i4\epsilon}{L})}{\eta(\frac{i4\epsilon}{L})}, & \text{Neumann B.C.} \\ \frac{\theta_3(0|\frac{i4\epsilon}{L})}{\eta(\frac{i4\epsilon}{L})}, & \text{Dirichlet B.C.} \end{cases} \tag{B3}$$

where $\theta_\nu(z|\tau)$ and $\eta(\tau)$ are the Jacobi theta functions and the Dedekind eta function which are described in some detail in [96]. Therefore, the correctly normalized Euclidean Rényi entanglement entropy to leading order in $\frac{L}{\epsilon}$ is

$$\begin{aligned}
S_{\mathcal{V}}^{(n)} = & -\frac{c}{24} \frac{n+1}{n} \log \left| \prod_{i=1,2} \left(\frac{dw_{v_i}^{\text{New},\alpha}}{dw_{v_i}} \right) \left(\frac{d\bar{w}_{v_i}^{\text{New},\alpha}}{d\bar{w}_{v_i}} \right) \right| \\
& + \frac{n+1}{12n} \log \left(\frac{L}{2\pi} \right)^2 \left| \left[\theta_1 \left(i \frac{w_{v_2}^{\text{New},\alpha} - w_{v_1}^{\text{New},\alpha}}{L} \middle| \frac{4i\epsilon}{L} \right) \theta_1 \left(i \frac{\bar{w}_{v_2}^{\text{New},\alpha} - \bar{w}_{v_1}^{\text{New},\alpha}}{L} \middle| \frac{4i\epsilon}{L} \right) \right. \right. \\
& \times \theta_1 \left(i \frac{w_{v_1}^{\text{New},\alpha} + \bar{w}_{v_1}^{\text{New},\alpha}}{L} \middle| \frac{4i\epsilon}{L} \right) \theta_1 \left(i \frac{w_{v_2}^{\text{New},\alpha} + \bar{w}_{v_2}^{\text{New},\alpha}}{L} \middle| \frac{4i\epsilon}{L} \right) \left. \right] \Big/ \left[\eta \left(i \frac{4\epsilon}{L} \right)^6 \right. \\
& \times \theta_1 \left(i \frac{w_{v_1}^{\text{New},\alpha} + \bar{w}_{v_2}^{\text{New},\alpha}}{L} \middle| \frac{4i\epsilon}{L} \right) \theta_1 \left(i \frac{w_{v_2}^{\text{New},\alpha} + \bar{w}_{v_1}^{\text{New},\alpha}}{L} \middle| \frac{4i\epsilon}{L} \right) \left. \right] \Big| \\
& + \begin{cases} \left[\frac{1}{1-n} \sum_{a=-\frac{n-1}{2}}^{\frac{n-1}{2}} \log \left| \theta_2 \left(i \frac{a(w_{v_1}^{\text{New},\alpha} - w_{v_2}^{\text{New},\alpha} + \bar{w}_{v_1}^{\text{New},\alpha} - \bar{w}_{v_2}^{\text{New},\alpha})}{Ln} \middle| \frac{4i\epsilon}{L} \right) \right. \right. \\ \left. \left. + \theta_3 \left(i \frac{a(w_{v_1}^{\text{New},\alpha} - w_{v_2}^{\text{New},\alpha} + \bar{w}_{v_1}^{\text{New},\alpha} - \bar{w}_{v_2}^{\text{New},\alpha})}{Ln} \middle| \frac{4i\epsilon}{L} \right) \right] \Big/ \left[\theta_2 \left(0 \middle| \frac{4i\epsilon}{L} \right) + \theta_3 \left(0 \middle| \frac{4i\epsilon}{L} \right) \right] \Big| & \text{Neumann} \\ \left[\frac{1}{1-n} \sum_{a=-\frac{n-1}{2}}^{\frac{n-1}{2}} \log \left| \theta_3 \left(i \frac{a(w_{v_1}^{\text{New},\alpha} - w_{v_2}^{\text{New},\alpha} + \bar{w}_{v_1}^{\text{New},\alpha} - \bar{w}_{v_2}^{\text{New},\alpha})}{Ln} \middle| \frac{4i\epsilon}{L} \right) \right. \right. \\ \left. \left. \Big/ \theta_3 \left(0 \middle| \frac{4i\epsilon}{L} \right) \right] \Big| & \text{Dirichlet} \end{cases} \quad \text{(B4)}
\end{aligned}$$

In this expression, as well as the subsequent expressions for Euclidean Rényi entropy and mutual information, the coordinates $w_{v_i}^{\text{New},\alpha}$ and $\bar{w}_{v_i}^{\text{New},\alpha}$ are analytically continued to real time, $\tau_1 \rightarrow it_1$. In the uniform $\theta = 0$ case with spatial periodicity $L = 2\pi$, we recover the corresponding expressions in [94,95]. The entanglement entropy for a boundary state at the initial time $t = 0$ for a subsystem of size $|\mathcal{V}| \gg \epsilon \rightarrow v_1 - v_2 \gg \epsilon$ in the limit where $L \gg \epsilon$ is given by

$$S_{\mathcal{V}}^{(n)}(t=0) = \frac{n+1}{6n} \log \frac{4\epsilon}{\pi} \quad \text{(B5)}$$

which does not depend on the total system and subsystem sizes since the boundary state possesses a low amount of

entanglement [68]. To compute the entanglement entropy of two intervals, the four-point function of the vertex operators is required. The calculation is a generalization of that in [94] and can be found in Appendix E.

If we have two intervals $A = [v_2, v_1]$ and $B = [v_4, v_3]$, then repeating the same calculation as for the single interval case gives

$$S_{AUB}^{(n)} = S_{AUB,\text{univ}}^{(n)} + S_{AUB,\text{nonuniv}}^{(n)} \quad \text{(B6)}$$

where the universal part that does not depend on the boundary condition is

$$\begin{aligned}
S_{AUB,\text{univ}}^{(n)} = & -\frac{c}{24} \frac{n+1}{n} \log \prod_{i=1}^4 \left| \frac{dw_{v_i}^{\text{New},\alpha}}{dw_{v_i}} \frac{d\bar{w}_{v_i}^{\text{New},\alpha}}{d\bar{w}_{v_i}} \right| + \frac{n+1}{12n} \log \left(\frac{L}{2\pi} \right)^4 \\
& \times \frac{\theta_1 \left(i \frac{w_{v_4}^{\text{New},\alpha} - w_{v_3}^{\text{New},\alpha}}{L} \middle| \frac{4i\epsilon}{L} \right) \theta_1 \left(i \frac{w_{v_4}^{\text{New},\alpha} - w_{v_1}^{\text{New},\alpha}}{L} \middle| \frac{4i\epsilon}{L} \right) \theta_1 \left(i \frac{w_{v_3}^{\text{New},\alpha} - w_{v_2}^{\text{New},\alpha}}{L} \middle| \frac{4i\epsilon}{L} \right) \theta_1 \left(i \frac{w_{v_2}^{\text{New},\alpha} - w_{v_1}^{\text{New},\alpha}}{L} \middle| \frac{4i\epsilon}{L} \right)}{\eta \left(\frac{4i\epsilon}{L} \right)^{12} \theta_1 \left(i \frac{w_{v_4}^{\text{New},\alpha} - w_{v_2}^{\text{New},\alpha}}{L} \middle| \frac{4i\epsilon}{L} \right) \theta_1 \left(i \frac{w_{v_3}^{\text{New},\alpha} - w_{v_1}^{\text{New},\alpha}}{L} \middle| \frac{4i\epsilon}{L} \right)} \\
& \times \frac{\theta_1 \left(i \frac{\bar{w}_{v_4}^{\text{New},\alpha} - \bar{w}_{v_3}^{\text{New},\alpha}}{L} \middle| \frac{4i\epsilon}{L} \right) \theta_1 \left(i \frac{\bar{w}_{v_4}^{\text{New},\alpha} - \bar{w}_{v_1}^{\text{New},\alpha}}{L} \middle| \frac{4i\epsilon}{L} \right) \theta_1 \left(i \frac{\bar{w}_{v_3}^{\text{New},\alpha} - \bar{w}_{v_2}^{\text{New},\alpha}}{L} \middle| \frac{4i\epsilon}{L} \right) \theta_1 \left(i \frac{\bar{w}_{v_2}^{\text{New},\alpha} - \bar{w}_{v_1}^{\text{New},\alpha}}{L} \middle| \frac{4i\epsilon}{L} \right)}{\theta_1 \left(i \frac{\bar{w}_{v_4}^{\text{New},\alpha} - \bar{w}_{v_2}^{\text{New},\alpha}}{L} \middle| \frac{4i\epsilon}{L} \right) \theta_1 \left(i \frac{\bar{w}_{v_3}^{\text{New},\alpha} - \bar{w}_{v_1}^{\text{New},\alpha}}{L} \middle| \frac{4i\epsilon}{L} \right)} \\
& \times \frac{\theta_1 \left(i \frac{w_{v_1}^{\text{New},\alpha} + \bar{w}_{v_1}^{\text{New},\alpha}}{L} \middle| \frac{4i\epsilon}{L} \right) \theta_1 \left(i \frac{w_{v_1}^{\text{New},\alpha} + \bar{w}_{v_3}^{\text{New},\alpha}}{L} \middle| \frac{4i\epsilon}{L} \right) \theta_1 \left(i \frac{w_{v_2}^{\text{New},\alpha} + \bar{w}_{v_2}^{\text{New},\alpha}}{L} \middle| \frac{4i\epsilon}{L} \right) \theta_1 \left(i \frac{w_{v_2}^{\text{New},\alpha} + \bar{w}_{v_4}^{\text{New},\alpha}}{L} \middle| \frac{4i\epsilon}{L} \right)}{\theta_1 \left(i \frac{w_{v_1}^{\text{New},\alpha} + \bar{w}_{v_2}^{\text{New},\alpha}}{L} \middle| \frac{4i\epsilon}{L} \right) \theta_1 \left(i \frac{w_{v_1}^{\text{New},\alpha} + \bar{w}_{v_4}^{\text{New},\alpha}}{L} \middle| \frac{4i\epsilon}{L} \right) \theta_1 \left(i \frac{w_{v_2}^{\text{New},\alpha} + \bar{w}_{v_1}^{\text{New},\alpha}}{L} \middle| \frac{4i\epsilon}{L} \right) \theta_1 \left(i \frac{w_{v_2}^{\text{New},\alpha} + \bar{w}_{v_3}^{\text{New},\alpha}}{L} \middle| \frac{4i\epsilon}{L} \right)} \\
& \times \frac{\theta_1 \left(i \frac{w_{v_3}^{\text{New},\alpha} + \bar{w}_{v_3}^{\text{New},\alpha}}{L} \middle| \frac{4i\epsilon}{L} \right) \theta_1 \left(i \frac{w_{v_3}^{\text{New},\alpha} + \bar{w}_{v_1}^{\text{New},\alpha}}{L} \middle| \frac{4i\epsilon}{L} \right) \theta_1 \left(i \frac{w_{v_4}^{\text{New},\alpha} + \bar{w}_{v_2}^{\text{New},\alpha}}{L} \middle| \frac{4i\epsilon}{L} \right) \theta_1 \left(i \frac{w_{v_4}^{\text{New},\alpha} + \bar{w}_{v_4}^{\text{New},\alpha}}{L} \middle| \frac{4i\epsilon}{L} \right)}{\theta_1 \left(i \frac{w_{v_3}^{\text{New},\alpha} + \bar{w}_{v_2}^{\text{New},\alpha}}{L} \middle| \frac{4i\epsilon}{L} \right) \theta_1 \left(i \frac{w_{v_3}^{\text{New},\alpha} + \bar{w}_{v_4}^{\text{New},\alpha}}{L} \middle| \frac{4i\epsilon}{L} \right) \theta_1 \left(i \frac{w_{v_4}^{\text{New},\alpha} + \bar{w}_{v_1}^{\text{New},\alpha}}{L} \middle| \frac{4i\epsilon}{L} \right) \theta_1 \left(i \frac{w_{v_4}^{\text{New},\alpha} + \bar{w}_{v_3}^{\text{New},\alpha}}{L} \middle| \frac{4i\epsilon}{L} \right)} \quad \text{(B7)}
\end{aligned}$$

and the nonuniversal part that depends on the boundary condition is

$$S_{AUB, \text{nonuniv}}^{(n)} = \begin{cases} \frac{1}{1-n} \sum_{a=-\frac{n-1}{2}}^{\frac{n-1}{2}} \log \left| \left[\theta_2 \left(i \frac{a}{n} \frac{w_{v_1}^{\text{New}, \alpha} - w_{v_2}^{\text{New}, \alpha} + w_{v_3}^{\text{New}, \alpha} - w_{v_4}^{\text{New}, \alpha} + \bar{w}_{v_1}^{\text{New}, \alpha} - \bar{w}_{v_2}^{\text{New}, \alpha} + \bar{w}_{v_3}^{\text{New}, \alpha} - \bar{w}_{v_4}^{\text{New}, \alpha}}{L} \middle| \frac{4i\epsilon}{L} \right) \right. \right. \\ \left. \left. + \theta_3 \left(i \frac{a}{n} \frac{w_{v_1}^{\text{New}, \alpha} - w_{v_2}^{\text{New}, \alpha} + w_{v_3}^{\text{New}, \alpha} - w_{v_4}^{\text{New}, \alpha} + \bar{w}_{v_1}^{\text{New}, \alpha} - \bar{w}_{v_2}^{\text{New}, \alpha} + \bar{w}_{v_3}^{\text{New}, \alpha} - \bar{w}_{v_4}^{\text{New}, \alpha}}{L} \middle| \frac{4i\epsilon}{L} \right) \right] \right. \\ \left. / \left[\theta_2 \left(\frac{4i\epsilon}{L} \right) + \theta_3 \left(\frac{4i\epsilon}{L} \right) \right] \right|, & \text{N} \\ \frac{1}{1-n} \sum_{a=-\frac{n-1}{2}}^{\frac{n-1}{2}} \log \left| \frac{\theta_3 \left(i \frac{a}{n} \frac{w_{v_1}^{\text{New}, \alpha} - w_{v_2}^{\text{New}, \alpha} + w_{v_3}^{\text{New}, \alpha} - w_{v_4}^{\text{New}, \alpha} + \bar{w}_{v_1}^{\text{New}, \alpha} - \bar{w}_{v_2}^{\text{New}, \alpha} + \bar{w}_{v_3}^{\text{New}, \alpha} - \bar{w}_{v_4}^{\text{New}, \alpha}}{L} \middle| \frac{4i\epsilon}{L} \right)}{\theta_3 \left(\frac{4i\epsilon}{L} \right)} \right|, & \text{D} \end{cases} \quad (\text{B8})$$

where N and D stand for the Neumann and Dirichlet boundary conditions, respectively.

2. Entanglement entropy for the single interval in 2D holographic CFT

Now, we turn to the details of the computation on entanglement entropy for the single interval in 2D holographic CFT.

a. Method of image

In this paper, we employ the method of images to compute the Euclidean Rényi entanglement entropy for the holographic CFTs, and then analytically continue to real time. Consider (2.11) for the single interval in this method. In this method, the two point function for the boundary state is given by the four point function of the original operators and their images. In the von Neumann limit, $n \rightarrow 1$, the Euclidean entanglement entropy is given by

$$\begin{aligned} S_{E, \mathcal{V}} &= \lim_{n \rightarrow 1} \frac{h_n}{1-n} \log \left[\left(\frac{dw_{v_1}^{\text{New}, \alpha}}{dw_{v_1}} \right) \left(\frac{d\bar{w}_{v_1}^{\text{New}, \alpha}}{d\bar{w}_{v_1}} \right) \left(\frac{dw_{v_2}^{\text{New}, \alpha}}{dw_{v_2}} \right) \left(\frac{d\bar{w}_{v_2}^{\text{New}, \alpha}}{d\bar{w}_{v_2}} \right) \right] \\ &+ \lim_{n \rightarrow 1} \frac{1}{2(1-n)} \log \left[\left\langle \bar{\mathcal{T}}_n \left(4\epsilon - \tau_{v_1, \tau_1, \alpha} + i \frac{L\varphi_{v_1, \tau_1, \alpha}}{2\pi}, 4\epsilon - \tau_{v_1, \tau_1, \alpha} + i \frac{L\bar{\varphi}_{v_1, \tau_1, \alpha}}{2\pi} \right) \right. \right. \\ &\times \mathcal{T}_n \left(4\epsilon - \tau_{v_2, \tau_1, \alpha} + i \frac{L\varphi_{v_2, \tau_1, \alpha}}{2\pi}, 4\epsilon - \tau_{v_2, \tau_1, \alpha} + i \frac{L\bar{\varphi}_{v_2, \tau_1, \alpha}}{2\pi} \right) \\ &\times \mathcal{T}_n \left(\tau_{v_1, \tau_1} + i \frac{L\varphi_{v_1, \tau_1}}{2\pi}, \tau_{v_1, \tau_1} + i \frac{L\bar{\varphi}_{v_1, \tau_1}}{2\pi} \right) \bar{\mathcal{T}}_n \left(\tau_{v_2, \tau_1, \alpha} + i \frac{L\varphi_{v_2, \tau_1, \alpha}}{2\pi}, \tau_{v_2, \tau_1, \alpha} + i \frac{L\bar{\varphi}_{v_2, \tau_1, \alpha}}{2\pi} \right) \left. \right\rangle_{\text{Torus}} \Big], \\ &= -\frac{c}{12} \log \left[\left(\frac{dw_{v_1}^{\text{New}, \alpha}}{dw_{v_1}} \right) \left(\frac{d\bar{w}_{v_1}^{\text{New}, \alpha}}{d\bar{w}_{v_1}} \right) \left(\frac{dw_{v_2}^{\text{New}, \alpha}}{dw_{v_2}} \right) \left(\frac{d\bar{w}_{v_2}^{\text{New}, \alpha}}{d\bar{w}_{v_2}} \right) \right] \\ &+ \lim_{n \rightarrow 1} \frac{1}{2(1-n)} \log \left[\left(\bar{\mathcal{T}}_n(3\epsilon - \bar{w}_{v_1}^{\text{New}, \alpha}, 3\epsilon - w_{v_1}^{\text{New}, \alpha}) \mathcal{T}_n(3\epsilon - \bar{w}_{v_2}^{\text{New}, \alpha}, 3\epsilon - w_{v_2}^{\text{New}, \alpha}) \right) \right. \\ &\times \mathcal{T}_n(\epsilon + w_{v_1}^{\text{New}, \alpha}, \epsilon + \bar{w}_{v_1}^{\text{New}, \alpha}) \bar{\mathcal{T}}_n(\epsilon + w_{v_2}^{\text{New}, \alpha}, \epsilon + \bar{w}_{v_2}^{\text{New}, \alpha}) \left. \right]_{\text{Torus}}, \end{aligned} \quad (\text{B9})$$

where the length of the thermal cycle is 4ϵ , and the mirrors are located at $\tau = 0$ and $\tau = 2\epsilon$. Here, $\tau_{v_i, \tau_1, \alpha}$ denotes the real part of $w_{v_i}^{\text{New}, \alpha}$ and $\bar{w}_{v_i}^{\text{New}, \alpha}$, while $\frac{L\varphi_{v_i, \tau_1, \alpha}}{2\pi}$ and $\frac{L\bar{\varphi}_{v_i, \tau_1, \alpha}}{2\pi}$ denote the imaginary parts, respectively. In the method of images, the geometry where the n -point functions are defined is a torus with thermal and spatial periods 4ϵ and L respectively. Here, n is an even integer. The first term in the last equation of (B9) is independent of the details of 2D CFTs, while the second term depends on those. We call the first and second terms the universal and nonuniversal

pieces, respectively. In 2D holographic CFTs, the nonuniversal piece is determined by the geodesic length in on the background dual of the system considered.

b. Nonuniversal piece in 2D holographic CFT

Now, we focus on the nonuniversal piece of the entanglement entropy in 2D holographic CFT. By employing the method of images, the system is equivalent to that on a spatial circle with circumference L in the thermal state with the inverse temperature $4\epsilon (\ll L)$. In other words, the

geometry where 2D CFTs live is the torus with 4ϵ and L . As explored in [97], in 2D holographic CFTs, the gravity dual of this system in the high temperature region, $\epsilon \ll L$, is given by the BTZ black hole, while that in the low temperature region, $\epsilon \gg L$, is given by the thermal AdS₃. Therefore, the nonuniversal piece in the high temperature region is given by the minimal length of geodesics in the BTZ black hole geometry [79,98]:

$$S_{\mathcal{V};\text{Nonuni}} = \text{Min}[S_{\mathcal{V};\text{con}}, S_{\mathcal{V};\text{dis}}], \quad (\text{B10})$$

where S_{con} is the length of geodesics connecting the points on the different Euclidean time slices, while S_{dis} is the length of geodesics connecting the points on the same Euclidean time slice. We present the details of S_{con} and S_{dis} , and they are given by

$$\begin{aligned} S_{\mathcal{V};\text{con}} &\approx \frac{c}{3} \log\left(\frac{4\epsilon}{\pi}\right) + \frac{c}{6} \times \left[\sum_{i=1,2} \log\left(\cos\left(\frac{\pi}{4\epsilon}(w_{v_i}^{\text{New},\alpha} + \bar{w}_{v_i}^{\text{New},\alpha})\right)\right) \right], \\ S_{\mathcal{V};\text{dis}} &\approx \frac{c}{3} \log\left(\frac{4\epsilon}{\pi}\right) + \text{Min}[S_{\mathcal{V};\text{dis},1}, S_{\mathcal{V};\text{dis},2}], \\ S_{\mathcal{V};\text{dis},1} &= \frac{c}{12} \log\left|\sin\left(\frac{\pi}{4\epsilon}(w_{v_1}^{\text{New},\alpha} - w_{v_2}^{\text{New},\alpha} \pm iL)\right)\right|^2 + \frac{c}{12} \log\left|\sin\left(\frac{\pi}{4\epsilon}(\bar{w}_{v_1}^{\text{New},\alpha} - \bar{w}_{v_2}^{\text{New},\alpha} \mp iL)\right)\right|^2, \\ S_{\mathcal{V};\text{dis},2} &= \frac{c}{12} \log\left|\sin\left(\frac{\pi}{4\epsilon}(w_{v_1}^{\text{New},\alpha} - w_{v_2}^{\text{New},\alpha})\right)\right|^2 + \frac{c}{12} \log\left|\sin\left(\frac{\pi}{4\epsilon}(\bar{w}_{v_1}^{\text{New},\alpha} - \bar{w}_{v_2}^{\text{New},\alpha})\right)\right|^2. \end{aligned} \quad (\text{B11})$$

APPENDIX C: EARLY-TIME EVOLUTION OF ENTANGLEMENT ENTROPY DURING THE MÖBIUS AND SSD EVOLUTION

We depict the early-time behavior of S_A as a function of t_1 in Fig. 11.

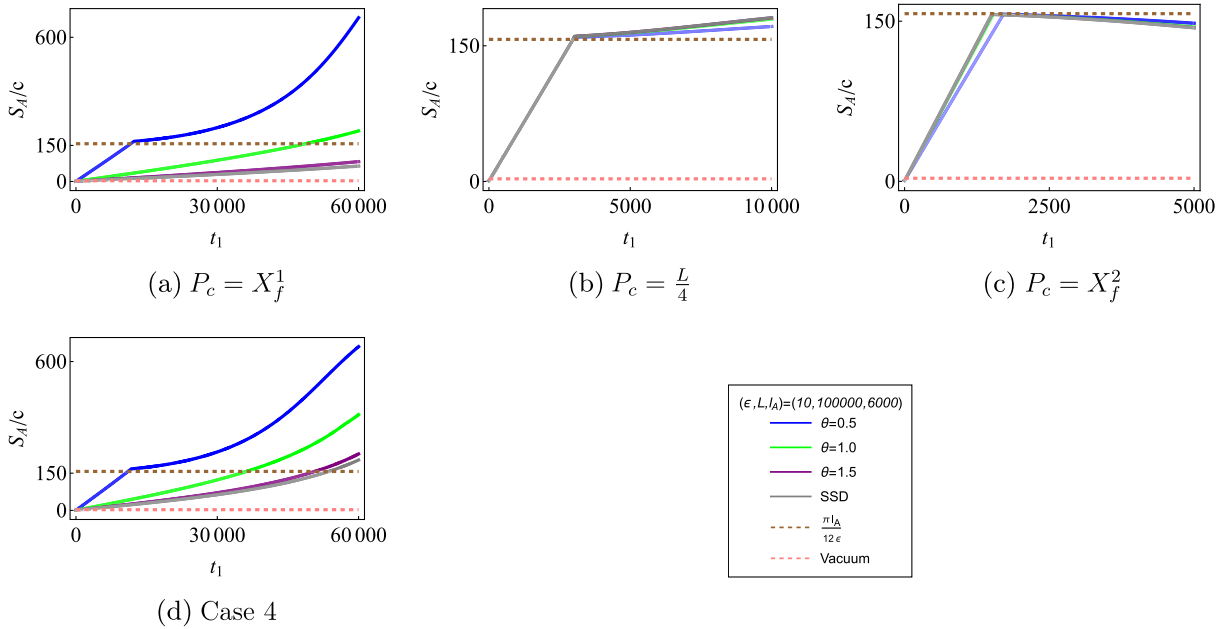


FIG. 11. The t_1 -dependence of S_A during the evolution induced by the Möbius and SSD Hamiltonians. The panels, [a], [b], [c], and [d] correspond to cases (1), (2), (3), and (4). Here, P_c denotes the center of A . For simplicity, in [a], [b], and [c], P_c is taken to be $P_c = X_f^1, L/4$, and X_f^2 , respectively. The blue, green, and purple curves illustrate the early time behavior of S_A during the Möbius evolution, while the gray line illustrates the early time behavior of S_A during the Möbius evolution. The brown and pink dashed lines illustrate S_A of the thermal state with 4ϵ , inverse temperature, and the vacuum state.

APPENDIX D: THE DEFINITION OF $\mathcal{L}_{A;\text{dis},i=1,2}$ AND $\mathcal{L}_{B;\text{dis},i=1,2}$

We report on the definition of $\mathcal{L}_{A;\text{dis},i=1,2}$ and $\mathcal{L}_{B;\text{dis},i=1,2}$, here. They are defined as

$$\mathcal{L}_{A;\text{dis},i} = \text{Min}[\mathcal{L}_{A;\text{dis},i}^{(1)}, \mathcal{L}_{A;\text{dis},i}^{(2)}], \mathcal{L}_{B;\text{dis},i} = \text{Min}[\mathcal{L}_{B;\text{dis},i}^{(1)}, \mathcal{L}_{B;\text{dis},i}^{(2)}], \quad (\text{D1})$$

where if $x = X_f^1$ is neither in A nor B , $\mathcal{L}_{\mathcal{V}=A,B;\text{dis},j=1,2}^{(i=1,2)}$ are respectively given by

$$\begin{aligned} \mathcal{L}_{A;\text{dis},1}^{(1)} &= \log \left| \sin \left(\frac{\pi}{4\epsilon} (w_{X_1}^{\text{New},\alpha} - w_{X_2}^{\text{New},\alpha} \pm iL) \right) \right|^2 + \log \left| \sin \left(\frac{\pi}{4\epsilon} (\bar{w}_{X_1}^{\text{New},\alpha} - \bar{w}_{X_2}^{\text{New},\alpha} \mp iL) \right) \right|^2, \\ \mathcal{L}_{A;\text{dis},1}^{(2)} &= \log \left| \sin \left(\frac{\pi}{4\epsilon} (w_{X_1}^{\text{New},\alpha} - w_{X_2}^{\text{New},\alpha}) \right) \right|^2 + \log \left| \sin \left(\frac{\pi}{4\epsilon} (-\bar{w}_{X_1}^{\text{New},\alpha} + \bar{w}_{X_2}^{\text{New},\alpha}) \right) \right|^2, \\ \mathcal{L}_{B;\text{dis},1}^{(1)} &= \log \left| \sin \left(\frac{\pi}{4\epsilon} (w_{Y_1}^{\text{New},\alpha} - w_{Y_2}^{\text{New},\alpha} \pm iL) \right) \right|^2 + \log \left| \sin \left(\frac{\pi}{4\epsilon} (\bar{w}_{Y_1}^{\text{New},\alpha} - \bar{w}_{Y_2}^{\text{New},\alpha} \mp iL) \right) \right|^2, \\ \mathcal{L}_{B;\text{dis},1}^{(2)} &= \log \left| \sin \left(\frac{\pi}{4\epsilon} (w_{Y_1}^{\text{New},\alpha} - w_{Y_2}^{\text{New},\alpha}) \right) \right|^2 + \log \left| \sin \left(\frac{\pi}{4\epsilon} (-\bar{w}_{Y_1}^{\text{New},\alpha} + \bar{w}_{Y_2}^{\text{New},\alpha}) \right) \right|^2, \\ \mathcal{L}_{A;\text{dis},2}^{(1)} &= \log \left| \sin \left(\frac{\pi}{4\epsilon} (w_{Y_2}^{\text{New},\alpha} - w_{X_1}^{\text{New},\alpha} \pm iL) \right) \right|^2 + \log \left| \sin \left(\frac{\pi}{4\epsilon} (-\bar{w}_{Y_2}^{\text{New},\alpha} + \bar{w}_{X_1}^{\text{New},\alpha} \mp iL) \right) \right|^2, \\ \mathcal{L}_{A;\text{dis},2}^{(2)} &= \log \left| \sin \left(\frac{\pi}{4\epsilon} (w_{Y_2}^{\text{New},\alpha} - w_{X_1}^{\text{New},\alpha}) \right) \right|^2 + \log \left| \sin \left(\frac{\pi}{4\epsilon} (-\bar{w}_{Y_2}^{\text{New},\alpha} + \bar{w}_{X_1}^{\text{New},\alpha}) \right) \right|^2, \\ \mathcal{L}_{B;\text{dis},2}^{(1)} &= \log \left| \sin \left(\frac{\pi}{4\epsilon} (w_{X_2}^{\text{New},\alpha} - w_{Y_1}^{\text{New},\alpha} \pm iL) \right) \right|^2 + \log \left| \sin \left(\frac{\pi}{4\epsilon} (\bar{w}_{X_2}^{\text{New},\alpha} - \bar{w}_{Y_1}^{\text{New},\alpha} \mp iL) \right) \right|^2, \\ \mathcal{L}_{B;\text{dis},2}^{(2)} &= \log \left| \sin \left(\frac{\pi}{4\epsilon} (w_{X_2}^{\text{New},\alpha} - w_{Y_1}^{\text{New},\alpha}) \right) \right|^2 + \log \left| \sin \left(\frac{\pi}{4\epsilon} (-\bar{w}_{X_2}^{\text{New},\alpha} + \bar{w}_{Y_1}^{\text{New},\alpha}) \right) \right|^2. \end{aligned} \quad (\text{D2})$$

If $x = X_f^1$ is in A , $\mathcal{L}_{\mathcal{V}=A,B;\text{dis},j=1}^{(i=1,2)}$ is the same as (D2), and $\mathcal{L}_{\mathcal{V}=A,B;\text{dis},j=2}^{(i=1,2)}$ are given by

$$\begin{aligned} \mathcal{L}_{A;\text{dis},2}^{(1)} &= \log \left| \sin \left(\frac{\pi}{4\epsilon} (w_{Y_2}^{\text{New},\alpha} - w_{X_2}^{\text{New},\alpha} \pm iL) \right) \right|^2 + \log \left| \sin \left(\frac{\pi}{4\epsilon} (\bar{w}_{Y_2}^{\text{New},\alpha} - \bar{w}_{X_2}^{\text{New},\alpha} \mp iL) \right) \right|^2, \\ \mathcal{L}_{A;\text{dis},2}^{(2)} &= \log \left| \sin \left(\frac{\pi}{4\epsilon} (w_{Y_2}^{\text{New},\alpha} - w_{X_2}^{\text{New},\alpha}) \right) \right|^2 + \log \left| \sin \left(\frac{\pi}{4\epsilon} (-\bar{w}_{Y_2}^{\text{New},\alpha} + \bar{w}_{X_2}^{\text{New},\alpha}) \right) \right|^2, \\ \mathcal{L}_{B;\text{dis},2}^{(1)} &= \log \left| \sin \left(\frac{\pi}{4\epsilon} (w_{X_1}^{\text{New},\alpha} - w_{Y_1}^{\text{New},\alpha} \pm iL) \right) \right|^2 + \log \left| \sin \left(\frac{\pi}{4\epsilon} (\bar{w}_{X_1}^{\text{New},\alpha} - \bar{w}_{Y_1}^{\text{New},\alpha} \mp iL) \right) \right|^2, \\ \mathcal{L}_{B;\text{dis},2}^{(2)} &= \log \left| \sin \left(\frac{\pi}{4\epsilon} (w_{X_1}^{\text{New},\alpha} - w_{Y_1}^{\text{New},\alpha}) \right) \right|^2 + \log \left| \sin \left(\frac{\pi}{4\epsilon} (-\bar{w}_{X_1}^{\text{New},\alpha} + \bar{w}_{Y_1}^{\text{New},\alpha}) \right) \right|^2. \end{aligned} \quad (\text{D3})$$

APPENDIX E: VERTEX OPERATOR FOUR-POINT FUNCTION IN FREE DIRAC FERMION BOUNDARY STATE

In this section, we generalize the computation of the vertex operator two-point function in [94] to the four-point function that we use to compute the mutual information.

$$\langle B | e^{-2\epsilon H} V_{k_L, k_R}(y_1, \bar{y}_1) V_{l_L, l_R}(y_2, \bar{y}_2) V_{r_L, r_R}(y_3, \bar{y}_3) V_{q_L, q_R}(y_4, \bar{y}_4) | B \rangle \quad (\text{E1})$$

We normal order the vertex operator in the same way as in [94] with the position and momenta of the zero mode in the same exponent,

$$V_{k_L, k_R}(y, \bar{y}) = e^{ik_L(x_L + is_L p_L y) + ik_R(x_R + is_R p_R \bar{y})} \prod_{m>0} (e^{k_L \frac{\alpha_m}{m} e^{m y} + k_R \frac{\tilde{\alpha}_m}{m} e^{m \bar{y}}}) \prod_{m>0} (e^{-k_L \frac{\alpha_m}{m} e^{-m y} - k_R \frac{\tilde{\alpha}_m}{m} e^{-m \bar{y}}}). \quad (\text{E2})$$

The zero mode is ordered differently from [96] where the position and momentum coordinates are split between different exponentials. For Neumann boundary conditions, $k_L = -k_R = \frac{a}{N}$, while $k_L = k_R = \frac{a}{N}$ for Dirichlet boundary conditions. The symbols, s_L and s_R , are arbitrary signs that we have introduced in front of the zero mode momentum such that under a spatial translation $\sigma \rightarrow \sigma + 2\pi$, if $s_L = s_R = s$, the boson winds around the target manifold as $X(\sigma + 2\pi) = X(\sigma) + 2s\pi wR$ so that $s = 1$ has the same periodicity as in [99]. This is equivalent to flipping the sign of the zero mode in the Laurent expansion of the current $i\partial X$ which is an equally legitimate Laurent expansion. Following [94], we

also do not include any cocycle factors as explained in [99]. Since these cocycle factors do not depend on the coordinates y, \bar{y} , commuting them past the position operators can only give phases that are independent of the spacetime coordinate. Furthermore, as explained in [99], the cocycle factors only affect the relative signs of certain amplitudes but we are only considering a single correlation function.

Set $s_L = s_R = 1$. For Neumann boundary conditions, set $\mu = -1$, $k_L = -k_R = k = -l_L = l_R = r_L = -r_R = -q_L = q_R$. For Dirichlet boundary conditions, set $k_L = k_R = k = -l_L = -l_R = r_L = r_R = -q_L = -q_R$. A calculation similar to the one in [94] gives

$$\begin{aligned}
& \langle B | e^{-2\epsilon H} V_{k_L, k_R}(y_1, \bar{y}_1) V_{l_L, l_R}(y_2, \bar{y}_2) V_{r_L, r_R}(y_3, \bar{y}_3) V_{q_L, q_R}(y_4, \bar{y}_4) | B \rangle \\
&= \frac{1}{\eta\left(\frac{2i\epsilon}{\pi}\right)} \left[\frac{\eta\left(\frac{2i\epsilon}{\pi}\right)^{12} \theta_1\left(\frac{y_4 - y_2}{2\pi i} \middle| \frac{2i\epsilon}{\pi}\right) \theta_1\left(\frac{y_3 - y_1}{2\pi i} \middle| \frac{2i\epsilon}{\pi}\right)}{\theta_1\left(\frac{y_4 - y_3}{2\pi i} \middle| \frac{2i\epsilon}{\pi}\right) \theta_1\left(\frac{y_4 - y_1}{2\pi i} \middle| \frac{2i\epsilon}{\pi}\right) \theta_1\left(\frac{y_3 - y_2}{2\pi i} \middle| \frac{2i\epsilon}{\pi}\right) \theta_1\left(\frac{y_2 - y_1}{2\pi i} \middle| \frac{2i\epsilon}{\pi}\right)} \right. \\
&\quad \times \frac{\theta_1\left(\frac{\bar{y}_4 - \bar{y}_2}{2\pi i} \middle| \frac{2i\epsilon}{\pi}\right) \theta_1\left(\frac{\bar{y}_3 - \bar{y}_1}{2\pi i} \middle| \frac{2i\epsilon}{\pi}\right)}{\theta_1\left(\frac{\bar{y}_4 - \bar{y}_3}{2\pi i} \middle| \frac{2i\epsilon}{\pi}\right) \theta_1\left(\frac{\bar{y}_4 - \bar{y}_1}{2\pi i} \middle| \frac{2i\epsilon}{\pi}\right) \theta_1\left(\frac{\bar{y}_3 - \bar{y}_2}{2\pi i} \middle| \frac{2i\epsilon}{\pi}\right) \theta_1\left(\frac{\bar{y}_2 - \bar{y}_1}{2\pi i} \middle| \frac{2i\epsilon}{\pi}\right)} \\
&\quad \times \frac{\theta_1\left(\frac{y_1 + \bar{y}_2}{2\pi i} \middle| \frac{2i\epsilon}{\pi}\right) \theta_1\left(\frac{y_1 + \bar{y}_4}{2\pi i} \middle| \frac{2i\epsilon}{\pi}\right) \theta_1\left(\frac{y_2 + \bar{y}_1}{2\pi i} \middle| \frac{2i\epsilon}{\pi}\right) \theta_1\left(\frac{y_2 + \bar{y}_3}{2\pi i} \middle| \frac{2i\epsilon}{\pi}\right)}{\theta_1\left(\frac{y_1 + \bar{y}_1}{2\pi i} \middle| \frac{2i\epsilon}{\pi}\right) \theta_1\left(\frac{y_1 + \bar{y}_3}{2\pi i} \middle| \frac{2i\epsilon}{\pi}\right) \theta_1\left(\frac{y_2 + \bar{y}_2}{2\pi i} \middle| \frac{2i\epsilon}{\pi}\right) \theta_1\left(\frac{y_2 + \bar{y}_4}{2\pi i} \middle| \frac{2i\epsilon}{\pi}\right)} \\
&\quad \times \left. \frac{\theta_1\left(\frac{y_3 + \bar{y}_2}{2\pi i} \middle| \frac{2i\epsilon}{\pi}\right) \theta_1\left(\frac{y_3 + \bar{y}_4}{2\pi i} \middle| \frac{2i\epsilon}{\pi}\right) \theta_1\left(\frac{y_4 + \bar{y}_1}{2\pi i} \middle| \frac{2i\epsilon}{\pi}\right) \theta_1\left(\frac{y_4 + \bar{y}_3}{2\pi i} \middle| \frac{2i\epsilon}{\pi}\right)}{\theta_1\left(\frac{y_3 + \bar{y}_1}{2\pi i} \middle| \frac{2i\epsilon}{\pi}\right) \theta_1\left(\frac{y_3 + \bar{y}_3}{2\pi i} \middle| \frac{2i\epsilon}{\pi}\right) \theta_1\left(\frac{y_4 + \bar{y}_2}{2\pi i} \middle| \frac{2i\epsilon}{\pi}\right) \theta_1\left(\frac{y_4 + \bar{y}_4}{2\pi i} \middle| \frac{2i\epsilon}{\pi}\right)} \right] k^2 \\
&\quad \times \begin{cases} |\mathcal{N}|^2 \left[\theta_2\left(\frac{k(y_1 - y_2 + y_3 - y_4 + \bar{y}_1 - \bar{y}_2 + \bar{y}_3 - \bar{y}_4)}{2\pi i} \middle| \frac{2i\epsilon}{\pi}\right) + \theta_3\left(\frac{k(y_1 - y_2 + y_3 - y_4 + \bar{y}_1 - \bar{y}_2 + \bar{y}_3 - \bar{y}_4)}{2\pi i} \middle| \frac{2i\epsilon}{\pi}\right) \right] & \text{Neumann} \\ |\mathcal{N}'|^2 \theta_3\left(\frac{k(y_1 - y_2 + y_3 - y_4 + \bar{y}_1 - \bar{y}_2 + \bar{y}_3 - \bar{y}_4)}{2\pi i} \middle| \frac{2i\epsilon}{\pi}\right) & \text{Dirichlet} \end{cases} \quad (E3)
\end{aligned}$$

-
- [1] J. M. Maldacena, The large N limit of superconformal field theories and supergravity, *Adv. Theor. Math. Phys.* **2**, 231 (1998).
- [2] S. Ryu and T. Takayanagi, Holographic derivation of entanglement entropy from the anti de Sitter space/conformal field theory correspondence, *Phys. Rev. Lett.* **96**, 181602 (2006).
- [3] S. Ryu and T. Takayanagi, Aspects of holographic entanglement entropy, *J. High Energy Phys.* **08** (2006) 045.
- [4] A. Almheiri, X. Dong, and D. Harlow, Bulk locality and quantum error correction in AdS/CFT, *J. High Energy Phys.* **04** (2015) 163.
- [5] F. Pastawski, B. Yoshida, D. Harlow, and J. Preskill, Holographic quantum error-correcting codes: Toy models for the bulk/boundary correspondence, *J. High Energy Phys.* **06** (2015) 149.
- [6] S. Choi, Y. Bao, X.-L. Qi, and E. Altman, Quantum error correction in scrambling dynamics and measurement-induced phase transition, *Phys. Rev. Lett.* **125**, 030505 (2020).
- [7] Y. Li and M. P. A. Fisher, Statistical mechanics of quantum error correcting codes, *Phys. Rev. B* **103**, 104306 (2021).
- [8] P. Mitra, M. Ippoliti, R. N. Bhatt, S. L. Sondhi, and K. Agarwal, Cooling arbitrary near-critical systems using hyperbolic quenches, *Phys. Rev. B* **99**, 104308 (2019).
- [9] K. Agarwal, R. N. Bhatt, and S. L. Sondhi, Fast preparation of critical ground states using superluminal fronts, *Phys. Rev. Lett.* **120**, 210604 (2018).
- [10] D. J. Griffiths and E. G. Harris, Introduction to quantum mechanics, *Am. J. Phys.* **63**, 767 (1995).
- [11] A. P. Young, S. Knysh, and V. N. Smelyanskiy, Size dependence of the minimum excitation gap in the quantum adiabatic algorithm, *Phys. Rev. Lett.* **101**, 170503 (2008).

- [12] I. Hen and A. P. Young, Exponential complexity of the quantum adiabatic algorithm for certain satisfiability problems, *Phys. Rev. E* **84**, 061152 (2011).
- [13] E. Farhi, D. Gosset, I. Hen, A. W. Sandvik, P. Shor, A. P. Young, and F. Zamponi, Performance of the quantum adiabatic algorithm on random instances of two optimization problems on regular hypergraphs, *Phys. Rev. A* **86**, 052334 (2012).
- [14] A. del Campo, Shortcuts to adiabaticity by counterdiabatic driving, *Phys. Rev. Lett.* **111**, 100502 (2013).
- [15] C. Jarzynski, Generating shortcuts to adiabaticity in quantum and classical dynamics, *Phys. Rev. A* **88**, 040101 (2013).
- [16] S. J. Glaser, T. Schulte-Herbruggen, M. Sieveking, O. Schedletsky, N. C. Nielsen, O. W. Sørensen, and C. Griesinger, Unitary control in quantum ensembles: Maximizing signal intensity in coherent spectroscopy, *Science* **280**, 421 (1998).
- [17] D. Sels and A. Polkovnikov, Minimizing irreversible losses in quantum systems by local counterdiabatic driving, *Proc. Natl. Acad. Sci. U.S.A.* **114**, E3909 (2017).
- [18] S. van Frank *et al.*, Optimal control of complex atomic quantum systems, *Sci. Rep.* **6**, 34187 (2016).
- [19] J. Geng, Y. Wu, X. Wang, K. Xu, F. Shi, Y. Xie, X. Rong, and J. Du, Experimental time-optimal universal control of spin qubits in solids, *Phys. Rev. Lett.* **117**, 170501 (2016).
- [20] R. R. Agunetz, C. D. Hill, L. C. L. Hollenberg, S. Rogge, and M. Blaauuboer, Superadiabatic quantum state transfer in spin chains, *Phys. Rev. A* **95**, 012317 (2017).
- [21] A. Baksic, H. Ribeiro, and A. A. Clerk, Speeding up adiabatic quantum state transfer by using dressed states, *Phys. Rev. Lett.* **116**, 230503 (2016).
- [22] G. M. Rotskoff, G. E. Crooks, and E. Vanden-Eijnden, Geometric approach to optimal nonequilibrium control: Minimizing dissipation in nanomagnetic spin systems, *Phys. Rev. E* **95**, 012148 (2017).
- [23] G. C. Hegerfeldt, Driving at the quantum speed limit: Optimal control of a two-level system, *Phys. Rev. Lett.* **111**, 260501 (2013).
- [24] W. W. Ho and T. H. Hsieh, Efficient variational simulation of non-trivial quantum states, *SciPost Phys.* **6**, 029 (2019).
- [25] S. Bao, S. Kleer, R. Wang, and A. Rahmani, Optimal control of superconducting qubits using Pontryagin's minimum principle: Preparing a maximally entangled state with singular bang-bang protocols, *Phys. Rev. A* **97**, 062343 (2018).
- [26] Z.-C. Yang, A. Rahmani, A. Shabani, H. Neven, and C. Chamon, Optimizing variational quantum algorithms using Pontryagin's minimum principle, *Phys. Rev. X* **7**, 021027 (2017).
- [27] M. Bukov, A. G. R. Day, D. Sels, P. Weinberg, A. Polkovnikov, and P. Mehta, Reinforcement learning in different phases of quantum control, *Phys. Rev. X* **8**, 031086 (2018).
- [28] M. P. Zaletel, A. Kaufman, D. M. Stamper-Kurn, and N. Y. Yao, Preparation of low entropy correlated many-body states via conformal cooling quenches, *Phys. Rev. Lett.* **126**, 103401 (2021).
- [29] T.-L. Ho and Q. Zhou, Universal cooling scheme for quantum simulation, [arXiv:0911.5506](https://arxiv.org/abs/0911.5506).
- [30] X. Wen and J.-Q. Wu, Quantum dynamics in sine-square deformed conformal field theory: Quench from uniform to nonuniform conformal field theory, *Phys. Rev. B* **97**, 184309 (2018).
- [31] I. MacCormack, A. Liu, M. Nozaki, and S. Ryu, Holographic duals of inhomogeneous systems: The rainbow chain and the sine-square deformation model, *J. Phys. A* **52**, 505401 (2019).
- [32] K. Goto, M. Nozaki, K. Tamaoka, M. T. Tan, and S. Ryu, Non-equilibrating a black hole with inhomogeneous quantum quench (2021).
- [33] W. Berdanier, M. Kolodrubetz, R. Vasseur, and J. E. Moore, Floquet dynamics of boundary-driven systems at criticality, *Phys. Rev. Lett.* **118**, 260602 (2017).
- [34] X. Wen and J.-Q. Wu, Floquet conformal field theory, [arXiv:1805.00031](https://arxiv.org/abs/1805.00031).
- [35] R. Fan, Y. Gu, A. Vishwanath, and X. Wen, Emergent spatial structure and entanglement localization in floquet conformal field theory, *Phys. Rev. X* **10**, 031036 (2020).
- [36] B. Han and X. Wen, Classification of SL_2 deformed floquet conformal field theories, *Phys. Rev. B* **102**, 205125 (2020).
- [37] X. Wen, R. Fan, A. Vishwanath, and Y. Gu, Periodically, quasiperiodically, and randomly driven conformal field theories, *Phys. Rev. Res.* **3**, 023044 (2021).
- [38] R. Fan, Y. Gu, A. Vishwanath, and X. Wen, Floquet conformal field theories with generally deformed Hamiltonians, *SciPost Phys.* **10**, 049 (2021).
- [39] X. Wen, Y. Gu, A. Vishwanath, and R. Fan, Periodically, quasi-periodically, and randomly driven conformal field theories (II): Furstenberg's theorem and exceptions to heating phases, *SciPost Phys.* **13**, 082 (2022).
- [40] B. Lapiere and P. Moosavi, Geometric approach to inhomogeneous floquet systems, *Phys. Rev. B* **103**, 224303 (2021).
- [41] B. Lapiere, K. Choo, C. Tauber, A. Tiwari, T. Neupert, and R. Chitra, Emergent black hole dynamics in critical floquet systems, *Phys. Rev. Res.* **2**, 023085 (2020).
- [42] P. Moosavi, Inhomogeneous conformal field theory out of equilibrium, *Ann. Henri Poincaré* (2021).
- [43] E. Langmann and P. Moosavi, Diffusive heat waves in random conformal field theory, *Phys. Rev. Lett.* **122**, 020201 (2019).
- [44] J. Dubail, J.-M. Stéphan, and P. Calabrese, Emergence of curved light-cones in a class of inhomogeneous Luttinger liquids, *SciPost Phys.* **3**, 019 (2017).
- [45] K. Gawędzki, E. Langmann, and P. Moosavi, Finite-time universality in nonequilibrium CFT, *J. Stat. Phys.* **172**, 353 (2018).
- [46] J. Dubail, J.-M. Stéphan, J. Viti, and P. Calabrese, Conformal field theory for inhomogeneous one-dimensional quantum systems: The example of non-interacting Fermi gases, *SciPost Phys.* **2**, 002 (2017).
- [47] T. Hikihara and T. Nishino, Connecting distant ends of one-dimensional critical systems by a sine-square deformation, *Phys. Rev. B* **83**, 060414 (2011).
- [48] A. Gendiar, R. Krmar, and T. Nishino, Spherical deformation for one-dimensional quantum systems, *Prog. Theor. Phys.* **122**, 953 (2009).

- [49] A. Gendiar, M. Daniška, Y. Lee, and T. Nishino, Suppression of finite-size effects in one-dimensional correlated systems, *Phys. Rev. A* **83**, 052118 (2011).
- [50] I. Maruyama, H. Katsura, and T. Hikihara, Sine-square deformation of free fermion systems in one and higher dimensions, *Phys. Rev. B* **84**, 165132 (2011).
- [51] H. Katsura, Sine-square deformation of solvable spin chains and conformal field theories, *J. Phys. A* **45**, 115003 (2012).
- [52] N. Ishibashi and T. Tada, Infinite circumference limit of conformal field theory, *J. Phys. A* **48**, 315402 (2015).
- [53] N. Ishibashi and T. Tada, Dipolar quantization and the infinite circumference limit of two-dimensional conformal field theories, *Int. J. Mod. Phys. A* **31**, 1650170 (2016).
- [54] K. Okunishi, Sine-square deformation and Mobius quantization of two-dimensional conformal field theory, *Prog. Theor. Exp. Phys.* **2016**, 063A02 (2016).
- [55] S. Tamura and H. Katsura, Zero-energy states in conformal field theory with sine-square deformation, *Prog. Theor. Exp. Phys.* **2017**, 113A01 (2017).
- [56] T. Tada, Conformal quantum mechanics and sine-square deformation, *Prog. Theor. Exp. Phys.* **2018**, 061B01 (2018).
- [57] R. Fan, Y. Gu, A. Vishwanath, and X. Wen, Floquet conformal field theories with generally deformed Hamiltonians, *SciPost Phys.* **10**, 049 (2021).
- [58] X. Wen and J.-Q. Wu, Floquet conformal field theory (2018).
- [59] K. Goto, M. Nozaki, S. Ryu, K. Tamaoka, and M. T. Tan, Scrambling and recovery of quantum information in inhomogeneous quenches in two-dimensional conformal field theories (2023).
- [60] J. de Boer, V. Godet, J. Kastikainen, and E. Keski-Vakkuri, Quantum information geometry of driven CFTs (2023).
- [61] P. Caputa and D. Ge, Entanglement and geometry from subalgebras of the Virasoro algebra, *J. High Energy Phys.* **06** (2023) 159.
- [62] S. Datta, B. Lapierre, P. Moosavi, and A. Tiwari, Marginal quenches and drives in Tomonaga-Luttinger liquids, *SciPost Phys.* **14**, 108 (2023).
- [63] J. Kudler-Flam, M. Nozaki, T. Numasawa, S. Ryu, and M. T. Tan, Bridging two quantum quench problems—local joining quantum quench and Möbius quench—and their holographic dual descriptions (2023).
- [64] X. Liu, A. McDonald, T. Numasawa, B. Lian, and S. Ryu, Quantum quenches of conformal field theory with open boundary (2023).
- [65] K. Goto, T. Guo, T. Nosaka, M. Nozaki, S. Ryu, and K. Tamaoka, Spatial deformation of many-body quantum chaotic systems and quantum information scrambling (2023).
- [66] X. Wen, R. Fan, and A. Vishwanath, Floquet’s refrigerator: Conformal cooling in driven quantum critical systems (2022).
- [67] P. Calabrese and J. L. Cardy, Evolution of entanglement entropy in one-dimensional systems, *J. Stat. Mech.* (2005) P04010.
- [68] M. Miyaji, S. Ryu, T. Takayanagi, and X. Wen, Boundary states as holographic duals of trivial spacetimes, *J. High Energy Phys.* **05** (2015) 152.
- [69] N. Margolus and L. B. Levitin, The maximum speed of dynamical evolution, *Physica (Amsterdam)* **120D**, 188 (1998).
- [70] X. Wen and J.-Q. Wu, Quantum dynamics in sine-square deformed conformal field theory: Quench from uniform to nonuniform conformal field theory, *Phys. Rev. B* **97**, 184309 (2018).
- [71] X. Wen, R. Fan, A. Vishwanath, and Y. Gu, Periodically, quasi-periodically, and randomly driven conformal field theories: Part I (2021).
- [72] P. Calabrese and J. Cardy, Quantum quenches in $1+1$ dimensional conformal field theories, *J. Stat. Mech.* (2016) 064003.
- [73] V. Alba and P. Calabrese, Entanglement and thermodynamics after a quantum quench in integrable systems, *Proc. Natl. Acad. Sci. U.S.A.* **114**, 7947 (2017).
- [74] P. Calabrese and J. Cardy, Evolution of entanglement entropy in one-dimensional systems, *J. Stat. Mech.* (2005) P04010.
- [75] T. Takayanagi, Holographic dual of BCFT, *Phys. Rev. Lett.* **107**, 101602 (2011).
- [76] M. Fujita, T. Takayanagi, and E. Tonni, Aspects of AdS/BCFT, *J. High Energy Phys.* **11** (2011) 043.
- [77] T. Hartman and J. Maldacena, Time evolution of entanglement entropy from black hole interiors, *J. High Energy Phys.* **05** (2013) 014.
- [78] S. Ryu and T. Takayanagi, Aspects of holographic entanglement entropy, *J. High Energy Phys.* **08** (2006) 045.
- [79] S. Ryu and T. Takayanagi, Holographic derivation of entanglement entropy from AdS/CFT, *Phys. Rev. Lett.* **96**, 181602 (2006).
- [80] J. Haegeman, T. J. Osborne, H. Verschelde, and F. Verstraete, Entanglement renormalization for quantum fields in real space, *Phys. Rev. Lett.* **110**, 100402 (2013).
- [81] M. Nozaki, S. Ryu, and T. Takayanagi, Holographic geometry of entanglement renormalization in quantum field theories, *J. High Energy Phys.* **10** (2012) 193.
- [82] A. Mollabashi, M. Nozaki, S. Ryu, and T. Takayanagi, Holographic geometry of cMERA for quantum quenches and finite temperature, *J. High Energy Phys.* **03** (2014) 098.
- [83] K. Ohmori and Y. Tachikawa, Physics at the entangling surface, *J. Stat. Mech.* (2015) P04010.
- [84] Y. Kusuki and Z. Wei, AdS/BCFT from conformal bootstrap: Construction of gravity with branes and particles, *J. High Energy Phys.* **01** (2023) 108.
- [85] G. Vidal, Entanglement renormalization, *Phys. Rev. Lett.* **99**, 220405 (2007).
- [86] G. Vidal, Entanglement renormalization: An introduction, [arXiv:0912.1651](https://arxiv.org/abs/0912.1651).
- [87] G. Evenbly and G. Vidal, Quantum criticality with the multi-scale entanglement renormalization ansatz, [arXiv:1109.5334](https://arxiv.org/abs/1109.5334).
- [88] A. R. Chandra, J. de Boer, M. Flory, M. P. Heller, S. Hörtner, and A. Rolph, Cost of holographic path integrals, *SciPost Phys.* **14**, 061 (2023).
- [89] A. R. Chandra, J. de Boer, M. Flory, M. P. Heller, S. Hörtner, and A. Rolph, Spacetime as a quantum circuit, *J. High Energy Phys.* **04** (2021) 207.
- [90] A. M. Gainutdinov, J. L. Jacobsen, N. Read, H. Saleur, and R. Vasseur, Logarithmic conformal field theory: A lattice approach, *J. Phys. A* **46**, 494012 (2013).
- [91] W. Koo and H. Saleur, Representations of the Virasoro algebra from lattice models, *Nucl. Phys.* **B426**, 459 (1994).

- [92] A. Gainutdinov, N. Read, and H. Saleur, Continuum limit and symmetries of the periodic $g_{\mathcal{L}}(1|1)$ spin chain, *Nucl. Phys.* **B871**, 245 (2013).
- [93] R. Yoshii, S. Yamashika, and S. Tsuchiya, Entanglement propagation in thermalization of an isolated quantum system, *J. Phys. Soc. Jpn.* **91**, 054601 (2022).
- [94] T. Takayanagi and T. Ugajin, Measuring black hole formations by entanglement entropy via coarse-graining, *J. High Energy Phys.* **11** (2010) 054.
- [95] T. Takayanagi and T. Tsuda, Free fermion cyclic/symmetric orbifold CFTS and entanglement entropy, *J. High Energy Phys.* **12** (2022) 004.
- [96] P. Di Francesco, P. Mathieu, and D. Senechal, *Conformal Field Theory*, Graduate Texts in Contemporary Physics (Springer-Verlag, New York, 1997).
- [97] E. Witten, Anti-de Sitter space, thermal phase transition, and confinement in gauge theories, *Adv. Theor. Math. Phys.* **2**, 505 (1998).
- [98] M. Headrick, General properties of holographic entanglement entropy, *J. High Energy Phys.* **03** (2014) 085.
- [99] J. Polchinski, *String Theory*, Vol. 1 of Cambridge Monographs on Mathematical Physics (Cambridge University Press, Cambridge, England, 1998).